ISSN 0869-5911, Petrology, 2022, Vol. 30, No. 5, pp. 523–544. © Pleiades Publishing, Ltd., 2022.
Russian Text © The Author(s), 2022, published in Petrologiya, 2022, Vol. 30, No. 5, pp. 545–568.

Mineralogical, Geochemical, and Nd-Sr Isotope Characteristics of Amphibolites from the Alag-Khadny High-Pressure Complex (SW Mongolia): Intracontinental Rifting as a Precursor of Continental-Margin Subduction

S. Yu. Skuzovatov[a], *, M. A. Gornova[a], and A. A. Karimov[a]

[a] *Vinogradov Institute of Geochemistry, Russian Academy of Sciences, Siberian Branch, Irkutsk, Russia*
**e-mail: skuzovatov@igc.irk.ru*

Received December 15, 2021; revised February 10, 2022; accepted March 10, 2022

Abstract—Within subduction-accretion complexes, high-pressure rocks (blueschists, eclogites) are commonly juxtaposed with lower-grade rocks, which represent their retrograded counterparts or were involved into accretionary event at later stages, and thus characterize distinct stages of evolution of accretionary belts. In SW Mongolia, the Central Asian Orogenic Belt includes Neoproterozoic–Early Paleozoic paleosubduction complexes represented by eclogites and associated rocks of the Alag-Khadny accretionary complex. This paper reports the results of mineralogical, geochemical and isotopic studies of amphibolites from this complex, the geochemical nature and relationships of which with eclogites have been yet uncertain. The texture of the studied rocks varies from fine- and medium-grained granoblastic and nematoblastic amphibole–plagioclase–epidote rocks to medium-grained nematoblastic amphibole–epidote–albite–titanite amphibolites, which experienced intense recrystallization as a response to late deformations. Primary assemblages include pargasite and Mg-hornblende ($^{[B]}Na = 0.07–0.16$, $^{IV}Al = 0.79–1.69$, $^{[A]}(Na + K + 2Ca) = 0.14–0.64$, $^{[C]}(Al + Ti + Fe^{3+}) = 0.58–1.29$, $Fe^{2+}/(Fe^{2+} + Mg) = 0.18–0.46$ at $Fe^{3+}/(Fe^{3+}+Al) = 0.18–0.77$), low-to-medium-Ca plagioclase ($An_{24–36}$), and epidote–clinozoisite ($0.08 < X_{Fe^{3+}} < 0.16$), whereas the retrograde assemblage is represented by albite and Mg-hornblende. Calculations using amphibole composition and amphibole/amphibole–plagioclase thermobarometry revealed peak *P-T* conditions up to 570–630°C and 7–9 kbar ascribed to the high-*T* epidote-amphibolite facies with subsequent greenschist-facies retrogression. The major-element composition of the amphibolites corresponds to low-alkali moderate-Ti tholeiites, although their trace-element composition varies significantly from N-MORB to E-MORB-type basalts, which are variably enriched in LREE, Nb, Ta, Th, U, and show negative Eu and Ti anomalies due to fractionation of parental melts for precursor rocks. Isotopic composition of Nd ($\varepsilon_{Nd}(550)$ from +5.1 to –9.1) and Sr ($(^{87}Sr/^{86}Sr)_{550} = 0.7057–0.7097$) indicates distinct mainly moderately-depleted nature of mantle sources for the mafic rocks, but also highlights the involvement of "anomalous" mantle domains with unradiogenic Nd composition. The data supports that the precursor rocks of the amphibolites were formed during intracontinental extension of a continental margin, which was likely linked to opening of a limited Neoproterozoic oceanic basin with a subsequent Late Vendian–Early Cambrian convergence. The medium- to high-pressure metamorphism of amphibolites had similar *P-T* conditions to that of retrograde metamorphism of eclogites and associated metasediments and was directly related to the Early Paleozoic subduction-accretion metamorphism (~550–540 Ma), or results from the final accretion during the formation of a tectonic mélange zone between the Lake zone and Dzabkhan terrane (~515–490 Ma or younger).

Keywords: Central Asian Orogenic Belt, subduction, accretion, metamorphism, amphibolites, trace elements, Nd-Sr isotopes

DOI: 10.1134/S0869591122040051

INTRODUCTION

Subduction-accretion complexes formed on convergent plate margins are characterized by the presence of high-pressure rocks (eclogites and glaucophane schists) in association with serpentinite mélange, metasedimentary and felsic rocks (Ernst, 2005). In the Pacific-type (oceanic) paleosubduction complexes, the high-pressure rocks are usually represented by metamorphosed analogues of oceanic rocks (N-, T-, and E-MORB basalts associated with terrigenous, siliciclastic flysch metasediments, and abyssal clays), which are genetically related to the evolution of paleooceans of similar age. In contrast, paleozones of continental (Alpine-type) subduction demonstrate significant geochemical and age diversity of rocks involved in subduction. In some cases, rocks in poly-

metamorphic paleosubduction belts mark the transition from oceanic to continental subduction (Song et al., 2006; Zhang et al., 2013). Regardless of the type of subduction belts, they usually show a juxtaposition of rocks of different metamorphic grade. In particular, medium-grade metamafic rocks (amphibolites, garnet amphibolites) could represent both the retrogressed eclogites and rocks that did not experience significant subsidence. Therefore, the consideration of geochemical, isotope, and thermobarometric data is required to decipher the evolution of accretionary structures.

Within recently revealed high-pressure Alag-Khadny Complex in SW Mongolia (Štípská et al., 2010; Skuzovatov et al., 2018), eclogites are juxtaposed with orthogneisses and metasedimentary rocks showing signs of subduction metamorphism (Skuzovatov, 2021), as well as with lower grade metamorphic rocks (metacarbonates, amphibolites). Geochemical studies showed a common paleooceanic nature of metamafic rocks of the complex and thus, its formation in an intraoceanic setting in the Vendian–Early Cambrian (Štípská et al., 2010). However, this suggestion was not confirmed by more detailed isotope-geochemical studies (Skuzovatov et al., 2018). This work reports mineralogical-geochemical and isotope data on amphibolites exposed in the southern periphery of the eclogite-bearing complex. These rocks could represent previously unproved fragments of oceanic crust of the Neoproterozoic oceanic basin, which are spatially and genetically related to the tectonic evolution of high-grade rocks.

GEOLOGICAL STRUCTURE OF SW MONGOLIA AND STUDIED AREA

The Central Asian Fold Belt (CAFB) bordered by the Siberian, Tarim, and North China cratons characterizes the largest Phanerozoic crustal growth on Earth (Jahn et al., 2000; Sengör et al., 1993). The belt consists of terranes of different geodynamic nature, mainly of subduction-accretion complexes, microcontinents with Precambrian basement, and ophiolites. The CAFB was formed owing to the evolution and closure of the Paleoasian Ocean from Neoproterozoic to Permian (e.g., Kozakov et al., 2012; Yarmolyuk et al., 2006; Jahn et al., 2000; Sengör et al., 1993). The Mongolian segment of the CAFB is the central structure of the belt. Its western and southwestern parts exemplify the collage of high-grade Precambrian blocks, Paleozoic arcs, and accretionary complexes (Fig. 1a) (Yarmolyuk et a., 2006; Dobretsov et al., 2003; Khain et al., 2003; Kröner et al., 2010). Northern Mongolia is mainly made up of Early Paleozoic (Caledonian) complexes, which are separated from the Late Paleozoic (Hercynian) complexes of South Mongolia by the Main Mongolian Lineament (Tomurtogoo, 1997). The studied area is located in the western part of Gobi Altai, within the Lake Zone of the Vendian–Early Paleozoic ophiolites and subduction–accretion complexes (Rudnev et al., 2013; Matsumoto and Tomurtogoo, 2003) between the lineament and suture separating the Lake Zone from complexes of the Dzabkhan microcontinent and the Baidarik Block (Kozakov et al., 2007, 2012).

Field studies were carried out within the Zamtyn Range, 20 km northeast of the Chandman settlement (Fig. 1b). The detailed description of geological structure of the area was given for the first time in (Hanžl, Aichler, 2007) and in (Štípská et al., 2010). According to the cited materials, the lower levels of the structure are occupied by the high-grade rocks of the Zamtyn-Nuruu crystalline complex with U-Pb zircon ages varying from Neoproterozoic to Early Cambrian (948–541 Ma) (Hanžl and Aichler, 2007; Kröner et al., 2010; Buriánek et al., 2017). The basement complexes are unconformably overlain by volcanosedimentary and carbonate rocks of the Tsakhir-Uul Formation with Early Cambrian fauna (Kröner et al., 2010). Eclogites were initially identified as separate boudins up to a few hundreds meters in size among metasedimentary rocks and carbonates (Štípská et al., 2010; Skuzovatov et al., 2018), being confined to the block consisting of orthogneisses and metapelites (Alag-Khadny crystalline complex) (Štípská et al., 2010; Skuzovatov et al., 2018). Based on the T-MORB geochemical signatures, the high-grade rocks were ascribed to the accretionary complex of the Early Cambrian subduction paleozone thrust onto the crystalline rocks of the basement. Later models suggest that the sedimentary and magmatic protoliths of the rocks were formed in a setting of continental margin, which evolved from Early Neoproterozoic rifting (Skuzovatov et al., 2018) or suprasubduction-back arc magmatism (Buriánek et al., 2017) to the Early Caledonian subduction-accretionary stage (540–530 Ma). Metamorphic conditions of the eclogites (600–620°C, 19–21 kbar) are interpreted as a result of continental-margin subduction (Štípská et al., 2010; Sku-

Fig. 1. (a) Geological structure of the central segment of the Central Asian Fold Belt after (Kozakov et al., 2021). (1) Quaternary sediments; (2) Devonian–Carboniferous turbidite deposits; (3) undivided Paleozoic–Early Mesozoic volcanoplutonic complexes; (4) paleooceanic and island-arc Hercynides of the South Altai zone; (5) deposits of the continental slope and passive margin; (6) Late Caledonides of the Mongol-Altai zone; (7) Ediacaran–Lower Cambrian paleooceanic and island-arc complexes of the Lake Zone; (8) Ediacaran–Neoproterozoic ophiolites of the Bayankhongor zone; (9) Early Neoproterozoic paleooceanic and island-arc complexes; (10–15) proved and inferred blocks of crystalline rocks; (10) Early Precambrian, (11) undivided shelf and volcanic sequences of the Bayankhongor zone and metamorphic rocks of the South Khangay metamorphic belt (Late Neoproterozoic), (12) Early Neoproterozoic metamorphic complexes (exposed and inferred beneath cover), (13) Late Neoproterozoic metamorphic complexes, (14) Early Paleozoic metamorphic complexes, (15) Late Paleozoic metamorphic complexes; (16) tectonic boundaries, faults; (17) position of the studied object. (b) Geological scheme of the studied area (modified after Buriánek et al., 2017).

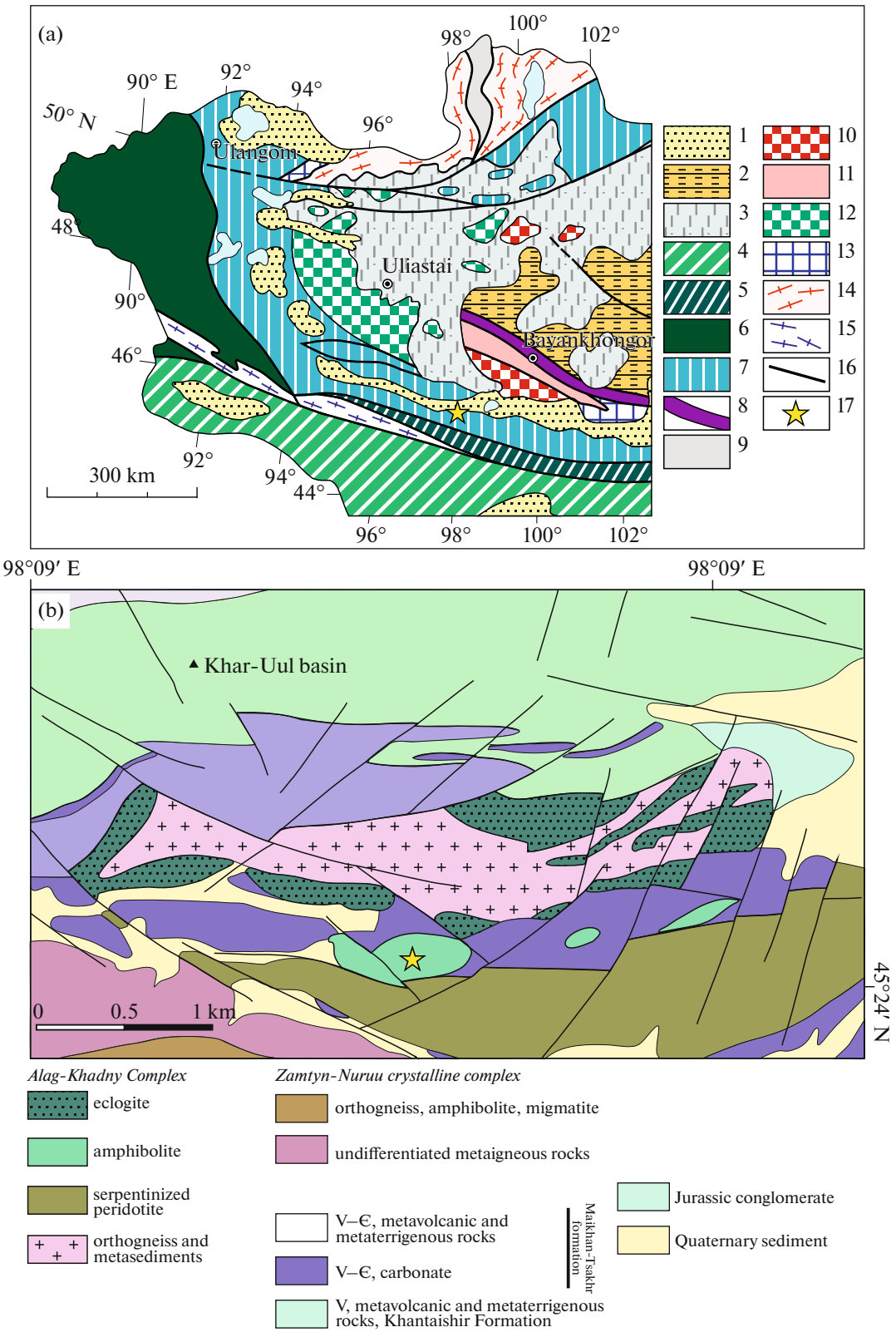
(a)
98°
100°
102°
90° E
92°
94°
96°
50° N
Ulangom
48°
Uliastai
90°
Bayankhongor
46°
92°
94°
300 km
44°
96°
98°
100°
102°
1
2
3
4
5
6
7
8
9
10
11
12
13
14
15
16
17
98°09′ E
98°09′ E
(b)
Khar-Uul basin
0
0.5
1 km
45°24′ N
Alag-Khadny Complex
eclogite
amphibolite
serpentinized peridotite
orthogneiss and metasediments
Zamtyn-Nuruu crystalline complex
orthogneiss, amphibolite, migmatite
undifferentiated metaigneous rocks
V–Є, metavolcanic and metaterrigenous rocks
V–Є, carbonate
Maikhan-Tsakhir formation
V, metavolcanic and metaterrigenous rocks, Khantaishir Formation
Jurassic conglomerate
Quaternary sediment

zovatov et al., 2018). The age of the eclogites and metapelites (Ar-Ar phengite age of 543 and 537 Ma, respectively) (Štípská et al., 2010) is similar to that of metamorphic zircons from orthogneisses (538 Ma) (Buriánek et al., 2017; Skuzovatov, 2021). Detailed *P-T* estimates for different lithologies associated with eclogites made it possible to establish the different degree of metamorphic transformation for the basement metagranitoids and metasedimentary schists (no more than 600–670°C and 11–14 kbar) and for metapelites (up to 500–570°C and 21–23 kbar), which likely had a common subduction history with eclogites. From the south, a zone of high-grade rocks is in a tectonic contact with Vendian–Early Cambrian carbonates of the Maikhan-Tsakhir Formation bearing amphibolite bodies, the development area of which is limited by metaperidotites from the south. Mineral assemblages and geochemical features of metaperidotites indicate that their protoliths were formed in an extensional setting, with subsequent suprasubduction refertilization by melts and/or fluids and metamorphism at *P-T* conditions similar to those of eclogite formation (640–720°C, 16–20 kbar) (Gornova et al., 2020).

ANALYTICAL METHODS

Sample preparation procedure and all analytical studies were conducted at the Center for Collective Use of Isotope-Geochemical Studies of the Vinogradov Institute of Geochemistry, Siberian Branch, Russian Academy of Sciences, Irkutsk. The compositions of rock-forming and accessory phases in amphibolites were acquired using a JEOL JXA8200 electron microprobe analyzer at a beam size of 2 μm, a beam current of 15 nA, and an accelerating voltage of 20 kV. The set of reference samples used for calibration involved albite (Na), pyrope garnet (Al), K-feldspar (K), diopside (Ca), forsterite (Mg), Mn-garnet (Mn), Ti-ilmenite (Ti) and Cr-spinel (Cr). Amphibole formulas were calculated according to the recommended classification using ACES algorithm (Amphibole Classification Excel Spreadsheet, version 1.9.8; Locock, 2014). Formula coefficients were calculated ignoring Ti^{4+} compensation by substitution of OH^- for O^{2-} in site W, which systematically underestimates Fe^{3+} by ~6–7%. Formulas for epidote–clinozoisite and plagioclase were calculated based on 8 cations and 16 charges (8 oxygen atoms), respectively, while titanite was calculated for 3 cations. Representative compositions of minerals from amphibolites of the Alag-Khadny Complex are given in Table 1; all data are given in Supplementary[1], ESM_1.xlsx.

[1] Supplementary materials to Russian and English on-line versions can be found at https://elibrary.ru/ and http://link.springer.com/, respectively:
ESM_1. xlsx—Compositions of minerals of epidote–clinozoisite amphibolites from the Alag-Khadny Complex, SW Mongolia.

To determine the bulk composition, rock fragments were ground in jaw crusher and powdered to 0.02 mm using steel mills. Major oxides were analyzed using X-ray fluorescence analysis on a Bruker S4 Pioneer spectrometer. The trace element contents were analyzed by ICP-MS method on a NexION 300D (Perkin Elmer) quadrupole mass-spectrometer with a preliminary sample preparation by open acid digestion. For both types of bulk analysis, standard samples (ST-1, SGD-1, BHVO-1) were used to control the accuracy and reproducibility of measurements.

For Sr and Nd isotope analyses by isotope dilution, whole-rock samples were spiked with ^{149}Sm-^{150}Nd and ^{85}Rb-^{84}Sr tracers and decomposed in a Savillex Teflon beakers in an $HF–HNO_3–HClO_4$ mixture (proportions of 3 : 1 : 0.3) in an ultrasonic bath, then evaporated on a plate at 100°C, and treated with 6 N HCl to remove formed fluorides and with 2 N HCl prior to applying to column. Sr was extracted in two stages by ion-exchange chromatography using BioRad AG 50W × 8 (200–400 mesh) and BioRad AG 50W × 12 (200–400 mesh) resins. The total REE and Sm-Nd were extracted using BioRad AG 50W × 12 (200–400 mesh) and LN-Resin (Eichrome) resins. The Sr isotope analysis was performed on a Finnigan MAT 262 thermoionization mass-spectrometer (TIMS) at the Geodynamics and Geochronology Center for Collective Use (Institute of the Earth's Crust, Siberian Branch of the Russian Academy of Sciences), in a static mode. Measured values were normalized to $^{88}Sr/^{86}Sr = 8.37521$ and controlled by replicate measurements of NBS-987 and BCR-2 standards. The Nd isotope analysis was conducted on a MC-ICP-MS Neptune Plus multicollector mass-spectrometer in static mode, and accuracy was controlled by replicate analysis of JNdi-1 and BCR-2 standards.

RESULTS

Petrography and Mineralogy of Rocks

Amphibolites form extended round bodies (from a few meters to 2 km long) in the carbonates of the Maikhan–Tsakhir Formation between zone of high-grade rocks and metaperidotites and are tectonic megaboudins. A spatial juxtaposition of eclogites and amphibolites are observed neither in carbonates south of the high-grade zone nor within the zone: the most retrograded eclogites are represented by apoeclogite garnet amphibolites. The rocks are made up of amphibole (40–70%), clinozoisite (20–30%), plagioclase (20–30%), sometimes quartz (up to 10%), and accessory titanite/rutile/titanomagnetite. They have gray-black color, banded structure, and fine to medium-grained texture and frequently contain sericite–calcite–chlorite veinlets. The petrographic study revealed a wide spectrum of characteristic textures and structures (Figs. 2, 3): from massive and fine-grained (grains up to 100 μm) granonematoblastic textures

Table 1. Representative compositons of minerals from amphibolites of the Alag-Khadny, SW Mongolia (wt %)

Compo-nents	Sample M16-36								Sample M16-37								Sample M16-41					
	*Amp*1	*Amp*2	*Ep*1	*Ep*2	*Pl*1	*Pl*2	Ti-*Mag*	Ti-*Mag*	*Amp*1	*Amp*2	*Ep*1	*Ep*2	*Pl*1	*Pl*2	*Rt*	*Ttn*	*Amp*1	*Amp*2	*Ep*1	*Ep*2	*Pl*1	*Pl*2
SiO_2	46.3	45.9	39.0	38.9	61.8	61.9	0.00	0.00	44.4	44.8	39.3	39.0	60.3	63.4	0.00	30.3	45.0	44.3	39.0	38.8	67.5	63.0
TiO_2	0.66	0.61	0.10	0.12	0.00	0.00	15.8	19.2	0.52	0.60	0.24	0.22	0.00	0.00	97.1	36.7	0.82	0.84	0.00	0.23	0.00	0.00
Al_2O_3	10.8	11.1	23.4	23.4	24.1	22.9	0.00	0.00	13.1	12.6	24.9	24.9	25.0	23.1	0.10	0.96	12.5	12.4	24.6	23.6	21.1	23.2
Cr_2O_3	0.00	0.00	0.00	0.00	0.00	0.00	0.00	0.00	0.00	0.00	0.00	0.00	0.00	0.00	0.00	0.00	0.00	0.00	0.00	0.00	0.00	0.00
FeO	15.5	15.4	12.1	12.2	0.21	0.17	77.7	74.1	15.8	15.6	10.4	10.4	0.37	0.20	0.69	0.60	15.5	15.5	11.0	12.0	0.34	0.31
MnO	0.33	0.34	0.16	0.16	0.00	0.00	0.61	0.23	0.27	0.28	0.13	0.16	0.00	0.00	0.00	0.00	0.29	0.26	0.15	0.17	0.00	0.00
MgO	12.4	12.4	0.00	0.00	0.00	0.00	0.00	0.00	11.3	11.5	0.00	0.00	0.00	0.00	0.00	0.00	11.5	12.0	0.00	0.00	0.00	0.00
CaO	11.5	11.6	23.1	23.1	6.28	5.03	0.00	0.00	11.3	11.3	23.1	23.4	7.30	4.55	0.40	28.6	11.4	11.4	23.4	23.5	1.13	4.73
Na_2O	1.83	2.02	0.00	0.00	7.75	8.43	0.13	0.00	1.85	2.22	0.00	0.00	7.15	8.69	0.00	0.00	2.17	2.09	0.00	0.00	9.95	8.74
K_2O	0.21	0.21	0.00	0.00	0.00	0.00	0.00	0.00	0.31	0.31	0.00	0.00	0.00	0.00	0.00	0.00	0.41	0.39	0.00	0.00	0.55	0.00
P_2O_5	0.00	0.00	0.00	0.00	0.00	0.00	0.00	0.00	0.00	0.00	0.00	0.00	0.00	0.00	0.00	0.20	0.00	0.00	0.00	0.00	0.00	0.00
Total	99.4	99.5	97.9	97.8	100.2	98.6	94.2	93.6	98.9	99.3	98.2	98.0	100.1	99.9	98.3	97.5	99.5	99.1	98.0	98.2	100.5	100.0
Si	6.66	6.60	3.06	3.06	2.75	2.76	0.00	0.00	6.44	6.50	3.07	3.05	2.68	2.82	0.00	1.01	6.51	6.41	3.05	3.04	3.00	2.80
Ti	0.07	0.07	0.01	0.01	0.00	0.00	0.61	0.76	0.06	0.07	0.01	0.01	0.00	0.00	0.98	0.92	0.09	0.09	0.00	0.01	0.00	0.00
Al	1.88	1.87	2.17	2.18	1.26	1.21	0.00	0.00	2.24	2.15	2.29	2.30	1.31	1.21	0.00	0.04	2.13	2.11	2.26	2.18	1.10	1.22
Fe^{2+}	1.45	1.44	0.12	0.10	0.01	0.01	0.00	0.00	1.46	1.66	0.14	0.09	0.01	0.01	0.00	0.00	1.67	1.39	0.08	0.07	0.01	0.01
Fe^{3+}	0.41	0.42	0.68	0.70	0.00	0.00	3.35	3.23	0.45	0.23	0.54	0.59	0.00	0.00	0.01	0.02	0.20	0.48	0.64	0.71	0.00	0.00
Mn	0.04	0.04	0.01	0.01	0.00	0.00	0.03	0.01	0.03	0.03	0.01	0.01	0.00	0.00	0.00	0.00	0.04	0.03	0.01	0.01	0.00	0.00
Mg	2.65	2.66	0.00	0.00	0.00	0.00	0.00	0.00	2.44	2.49	0.0	0.00	0.00	0.00	0.00	0.00	2.47	2.60	0.00	000	0.00	0.00
Ca	1.78	1.78	1.95	1.95	0.30	0.24	0.00	0.00	1.76	1.76	1.94	1.96	0.35	0.22	0.01	1.02	1.78	1.76	1.96	1.97	0.05	0.23
Na	0.54	0.55	0.00	0.00	0.67	0.73	0.01	0.00	0.52	0.62	0.00	0.00	0.62	0.75	0.00	0.00	0.61	0.59	0.00	0.00	0.86	0.75
K	0.04	0.04	0.00	0.00	0.00	0.00	0.00	0.00	0.06	0.06	0.00	0.00	0.00	0.00	0.00	0.00	0.08	0.07	0.00	0.00	0.03	0.00

Table 1. (Contd.)

Components	Sample M16-41	Sample M16-44					Sample M16-43								Sample M16-42						
	Ttn	*Amp*1	*Amp*2	*Ep*1	*Ep*2	*Rt*	*Amp*1	*Amp*2	*Ep*1	*Ep*2	*Pl*1	*Pl*2	*Ttn*	*Rt*	*Amp*1	*Amp*2	*Ep*1	*Ep*2	*Pl*1	*Pl*2	*Ttn*
SiO_2	31.3	43.3	44.1	39.5	39.6	0.00	45.7	44.9	39.3	38.9	67.5	59.2	31.2	0.00	46.5	49.6	39.4	39.0	62.6	67.7	31.2
TiO_2	37.4	0.69	0.65	0.13	0.15	95.5	0.58	0.67	0.00	0.14	0.00	0.00	36.3	93.8	0.53	0.44	0.10	0.00	0.00	0.00	38.1
Al_2O_3	0.81	14.5	14.1	26.1	26.7	0.00	11.1	10.2	23.2	23.9	20.7	25.6	1.16	0.00	11.2	8.76	24.9	22.7	23.5	20.3	0.71
Cr_2O_3	0.13	0.00	0.00	0.00	0.00	0.00	0.00	0.00	0.00	0.00	0.00	0.00	0.00	0.16	0.00	0.00	0.00	0.00	0.00	0.00	0.29
FeO	0.76	16.6	16.5	9.50	7.91	0.58	16.0	16.5	12.3	11.5	0.00	1.20	0.77	0.93	12.7	11.9	9.57	13.1	0.17	0.18	0.53
MnO	0.00	0.28	0.26	0.16	0.11	0.00	0.30	0.35	0.16	0.16	0.00	0.00	0.00	0.00	0.41	0.38	0.13	0.35	0.00	0.00	0.11
MgO	0.00	9.78	10.1	0.00	0.00	0.00	11.3	11.7	0.00	0.00	0.00	0.00	0.00	0.00	13.8	15.2	0.00	0.00	0.00	0.00	0.00
CaO	28.7	11.4	11.4	23.2	23.6	0.36	11.6	11.7	23.5	23.3	1.04	0.50	28.4	1.07	11.7	11.9	23.5	23.2	5.81	1.09	28.8
Na_2O	0.00	1.66	1.67	0.00	0.00	0.00	1.55	1.42	0.00	0.00	9.51	4.86	0.00	0.00	1.75	1.42	0.00	0.00	7.78	10.6	0.00
K_2O	0.00	0.58	0.62	0.00	0.00	0.00	1.10	1.12	0.00	0.00	0.28	5.08	0.00	0.00	0.31	0.25	0.00	0.00	0.11	0.00	0.00
P_2O_5	0.00	0.00	0.00	0.00	0.00	0.00	0.00	0.00	0.00	0.00	0.00	0.00	0.16	0.00	0.00	0.00	0.00	0.00	0.00	0.00	0.00
Total	99.1	98.7	99.3	98.5	98.1	96.4	99.3	98.5	98.4	97.9	99.1	96.4	98.0	95.9	99.0	99.9	97.7	98.2	99.9	99.7	99.7
Si	1.02	6.34	6.41	3.06	3.07	0.00	6.67	6.60	3.08	3.06	3.01	2.64	1.03	0.00	6.64	6.96	3.09	3.07	2.79	3.01	1.02
Ti	0.92	0.08	0.07	0.01	0.01	0.99	0.06	0.07	0.00	0.01	0.00	0.00	0.90	0.97	0.06	0.05	0.01	0.00	0.00	0.00	0.93
Al	0.03	2.50	2.41	2.38	2.44	0.00	1.91	1.77	2.14	2.21	1.09	1.34	0.05	0.00	1.89	1.45	2.30	2.10	1.23	1.06	0.03
Fe^{2+}	0.00	1.81	1.78	0.14	0.11	0.00	1.80	1.59	0.10	0.09	0.00	0.04	0.00	0.00	1.13	1.08	0.11	0.09	0.01	0.01	0.01
Fe^{3+}	0.02	0.23	0.23	0.48	0.40	0.01	0.16	0.43	0.71	0.66	0.00	0.00	0.02	0.01	0.39	0.33	0.52	0.77	0.00	0.00	0.01
Mn	0.00	0.03	0.03	0.01	0.01	0.00	0.04	0.04	0.01	0.01	0.00	0.00	0.00	0.00	0.05	0.05	0.01	0.02	0.00	0.00	0.00
Mg	0.00	2.14	2.20	0.00	0.00	0.00	2.45	2.56	0.00	0.00	0.00	0.00	0.00	0.00	2.94	3.19	0.00	0.00	0.00	0.00	0.00
Ca	1.01	1.79	1.77	1.92	1.96	0.01	1.82	1.85	1.97	1.96	0.05	0.02	1.00	0.02	1.80	1.79	1.98	1.95	0.28	0.05	1.00
Na	0.00	0.47	0.47	0.00	0.00	0.00	0.44	0.41	0.00	0.00	0.82	0.42	0.00	0.00	0.49	0.39	0.00	0.00	0.67	0.91	0.00
K	0.00	0.11	0.12	0.00	0.00	0.00	0.21	0.21	0.00	0.00	0.02	0.29	0.00	0.00	0.06	0.04	0.00	0.00	0.01	0.00	0.00

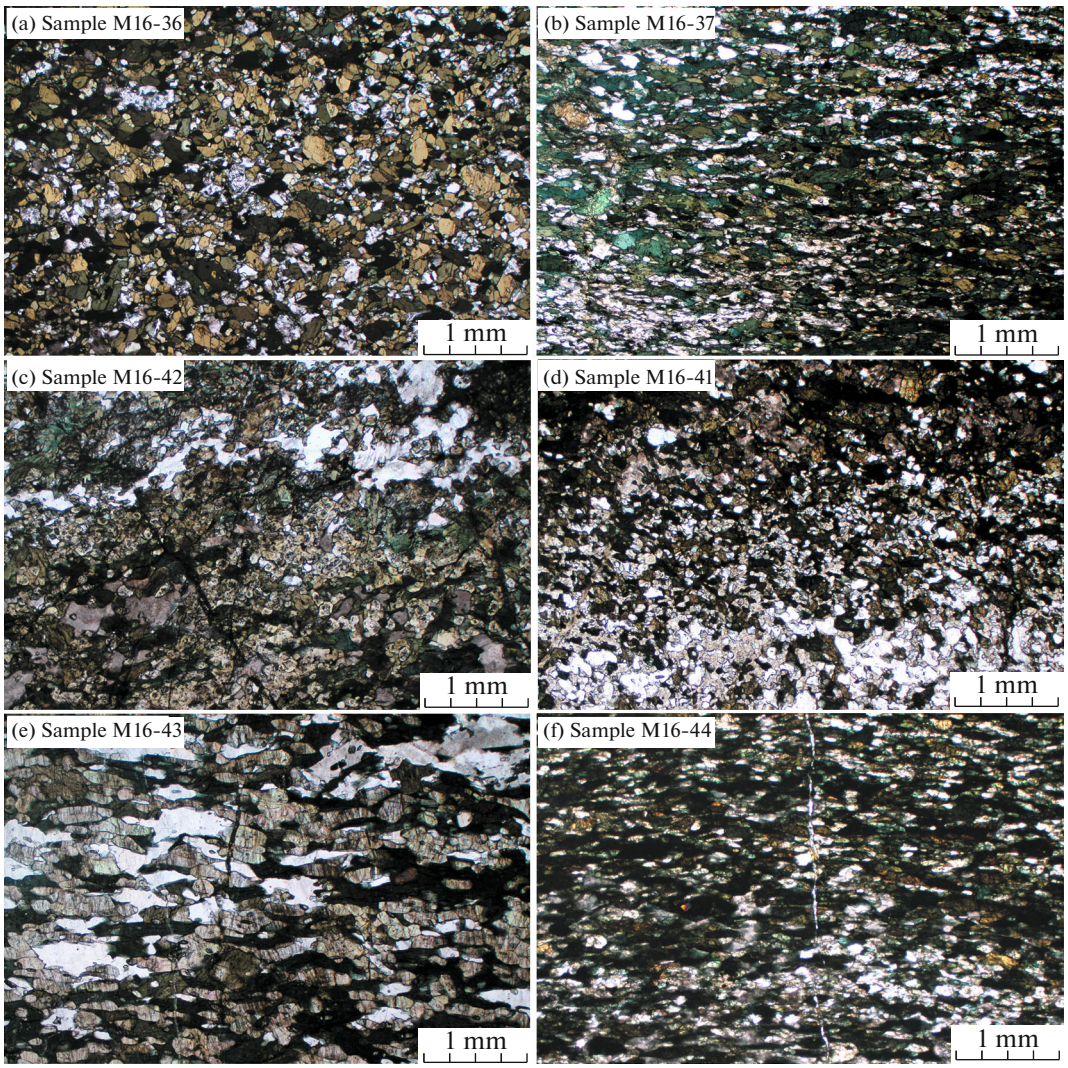

Fig. 2. Petrographic features of the studied epidote–clinozoisite amphibolites (in transmitted light).

with randomly oriented minerals (Figs. 2a, 2d; 3a, 3f) to nematoblastic and banded directive textures with subparallel orientation of amphibole and epidote–clinozoisite (Figs. 2b, 2e, 2f; 3c, 3e). In some amphibolites, banding is accompanied by a significant increase of grain size (up to 1–1.5 μm, Figs. 2e, 3e) of both rock-forming amphibole and epidote–clinozoisite, and accessory titanite. Signs of migmatization are not observed. Mineral abbreviations are given according to (Whitney and Evans, 2010).

Amphibole is ascribed to Ca-group and varies in composition from pargasite to magnesian hornblende ($^{[B]}$Na = 0.07–0.16, ^{IV}Al = 0.79–1.69) (Fig. 4a; given according to Tsujimori et al., 2006). According to amphibole classification (Hawthorne et al., 2012), data points fall mainly in the field of magnesian hornblende at $^{[A]}$(Na + K + 2Ca) = 0.14–0.64, $^{[C]}$(Al + Ti + Fe^{3+}) = 0.58–1.29 (Fig. 4b). Calculation for formula coefficients according to (Holland and Blundy, 1994) yields close results. The Ti content (0.02–0.10 a.p.f.u) changes insignificantly at wider variations of ^{IV}Al (see above) and ^{VI}Al (0.19–0.85 a.p.f.u.). Calculated Fe mole fraction (Fe^{2+}/(Fe^{2+} + Mg)) of the amphiboles is within 0.18–0.46 at Fe^{3+}/(Fe^{3+} + Al) = 0.18–0.77. The observed trends and compositional features are typical of metamorphic amphiboles from medium-grade metamafic rocks (Gerya et al., 1997; Zenk and Schulz, 2004; Schumacher, 2007) and indicate the absence of relicts of primary magmatic amphibole. In some samples, amphibole is azonal or weakly zoned, with cores represented by higher Ti and higher Al amphibole. This zoning is best expressed in samples M16-42 and M16-43 due to significant depletion of rims in Al, Na, and/or Ti (Fig. 4). Similar tendency together with general character and scales of compositional variations of amphibole in these samples suggests re-equilibration of primary amphibole–epi-

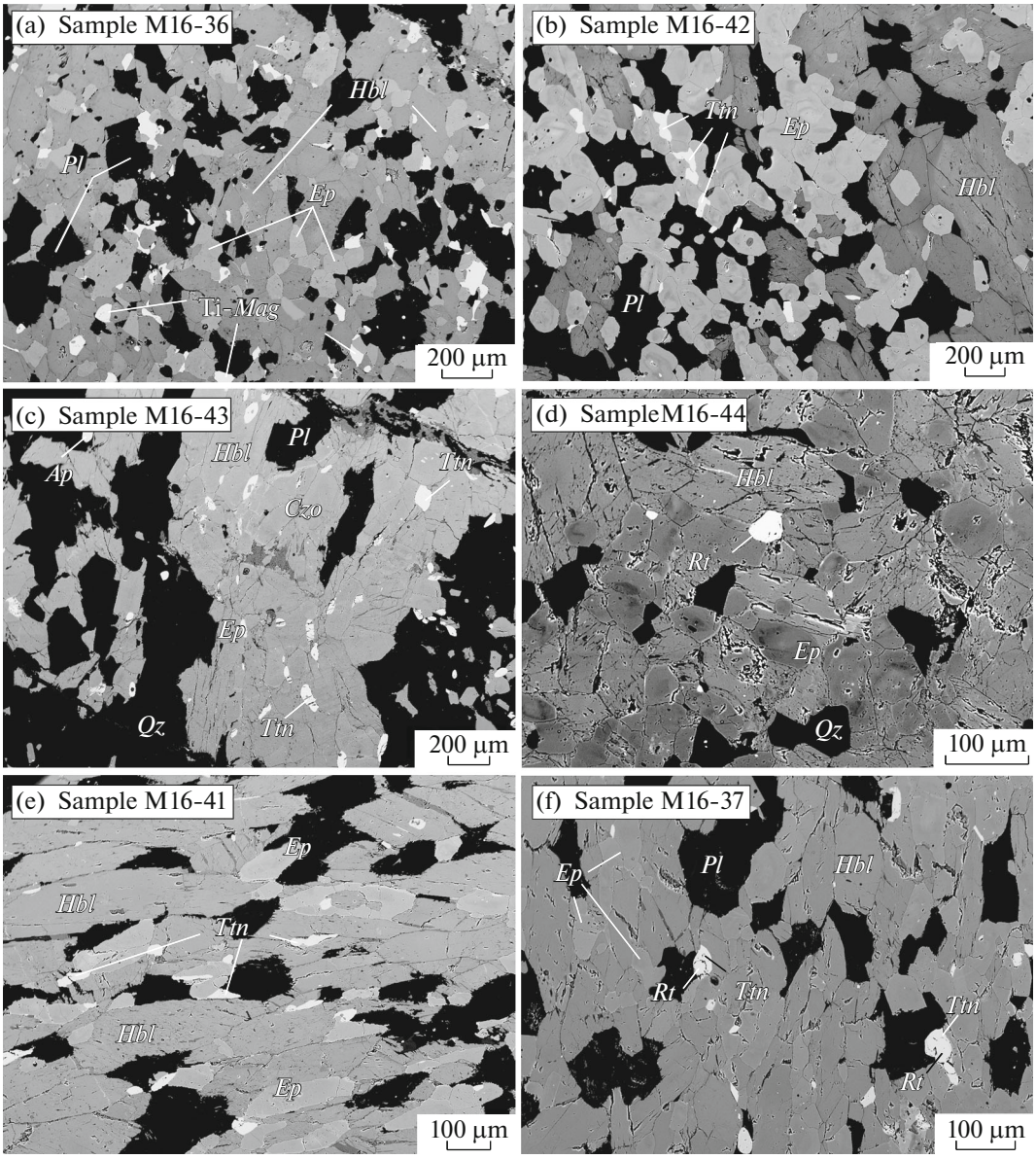

Fig. 3. Detailed structural relations of rock-forming and accessory minerals in amphibolites (BSE microimages).

dote–plagioclase assemblages under low-temperature epidote–amphibolite facies conditions.

Clinozoisite-group minerals vary in Fe mole fraction (Fe^{3+} = 0.37–0.77 a.p.f.u., $Fe^{3+}/(Fe^{3+} + Al)$ = 0.13–0.25, Fig. 5a) and are ascribed to epidotes, sometimes, to clinozoisites (Fe^{3+} = 0.4–0.5 a.p.f.u.). The epidote–clinozoisite contains 0.10–0.35 wt % MnO, demonstrates a homogenous distribution of pistazite end member or its outward growth (expressed, for instance, in pronounced zoning in BSE images in Fig. 3d).

Plagioclase reveals significant compositional variations (Fig. 5b). In samples showing no superimposed processes, plagioclase is represented by oligoclase–andesine ($An_{24–36}$). In many cases, the primary oligoclase–andesine is replaced by secondary plagioclase from higher Na composition to albite ($An_{2–10}$) or albite–epidote–sericite aggregate. Amphibolites containing mainly sodic plagioclase are characterized by the presence of quartz and mentioned above trend of amphibole toward the tremolite/ferroactinolite (higher SiO_2 and low Al_2O_3 and Na_2O).

Ti minerals in amphibolites are represented by accessory Ti-magnetite, rutile, and titanite. *Ti-magnetite* (13.2–19.2 wt % TiO_2) was found in one sample with most massive and fine-grained texture (sample M16-36, Fig. 2a). Two samples (M16-41, M16-42) contain *titanite* (0.80–1.80 wt % Al_2O_3) (Figs. 3e, 3b). Samples M16-37 and M16-43 contain rutile (0.56–0.93 wt % FeO) and titanite (0.96–1.33 wt % Al_2O_3,

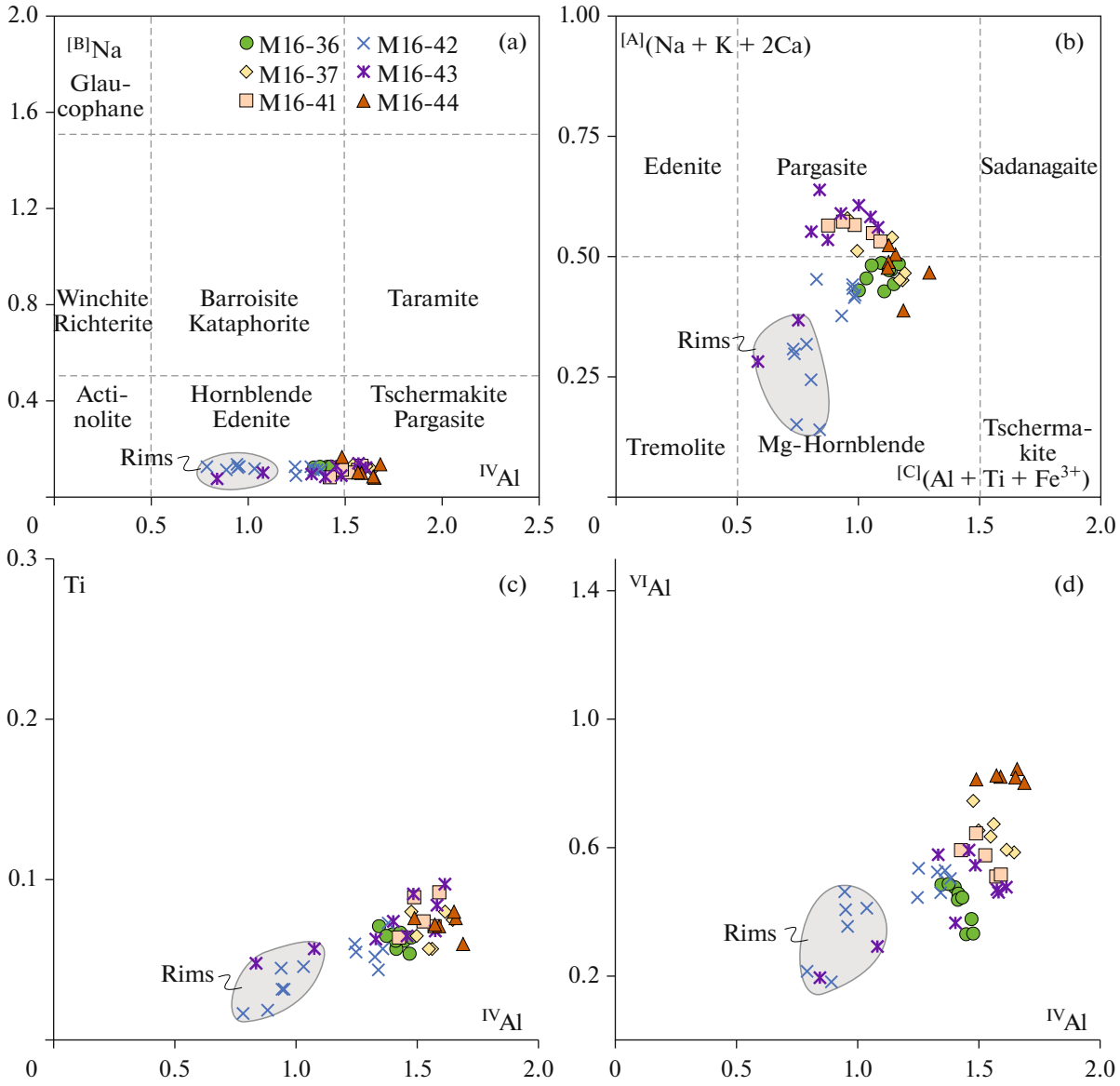

Fig. 4. Composition of amphiboles in the studied amphibolites.

0.13–0.17 wt % F, 0.13–0.20 wt % P_2O_5). Thereby, titanite occurs as separate grains and as replacement/overgrowth rims in rutile (Figs. 3c, 3f). Amphibole (sample M16-44) contains only rutile (Fig. 3d).

Mineral Thermobarometry

The medium-grade metamafic rocks have limited variations of modal composition (Oh and Liou, 1998), but demonstrate wide variations of zonal rock-forming phases, in particular, Ca-amphibole (Laird and Albee, 1981; Raase, 1994; Zenk and Schulz, 2004), which is an important source of information on the *P-T* evolution of the rocks. The composition of amphiboles, in particular, the degree of tschermakite and glaucophane isomorphism, depends on the metamorphic grade, which leads to the increase of Ti, ^{VI}Al, and $^{[A]}$Na contents with temperature increase and ^{VI}Al and $^{[M4]}$Na with pressure increase (Brown, 1977; Spear, 1980; Gerya et al., 1997; Ernst and Liu, 1998; Zenk and Schulz, 2004). In this paper, *P-T* parameters were estimated using amphibole–plagioclase geothermometer (Holland and Blundy, 1994). However, its application is limited by (1) the fact that free quartz involved in amphibole-forming reactions is present only in two samples, (2) ubiquitous replacement of primary plagioclase (presence of two plagioclase generations or the complete absence of andesine–oligoclase), and (3) potentially disequilibrium character of association of late amphibole with albite. This could result in the slightly overestimated temperature values (calculated for pressure of 7 kbar) on quartz-free

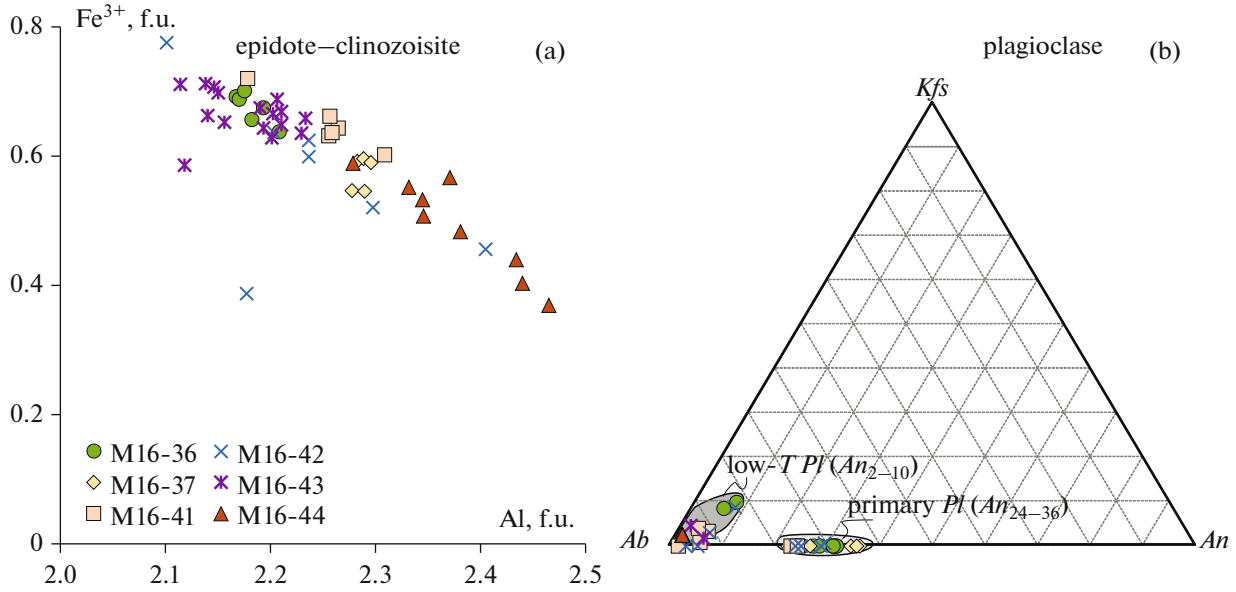

Fig. 5. Composition of epidote–clinozoisite (a) and plagioclase (b) in the studied amphibolites.

amphibolites (~690–750°C for sample M16-36, 650–730°C for sample M16-37, 680–710°C for sample M16-41) and slightly lower values of 640–690°C for sample M16-42 with single quartz grains. Incorrect estimates were obtained for quartz-bearing amphibolites (samples M16-43, M16-44) with albitic plagioclase. The series of *P-T* estimates obtained from amphibole composition using geothermobarometers according to (Gerya et al., 1997), in modified form after (Zenk and Schulz, 2004), are restricted to the relatively narrow range of more moderate temperatures (570–630°C) and pressures (4–7 kbar), except for lower parameters determined for low-Al and low-Ti rims of two samples M16-42 and M16-43 (500–550°C, 3–4 kbar) (Fig. 6).

Petro- and Geochemistry

The studied amphibolites are characterized by a sufficiently limited range of SiO_2 = 48.0–51.0 wt % and total alkalis ($K_2O + Na_2O$) = 2.07–2.85 wt %, low to moderate TiO_2 = 0.49–1.45 wt % and Mg# = 0.44–0.52, which correspond to low-Ti Fe-rich tholeiites (Table 2). The magnesian number (Mg# = 0.30–0.38) corresponds to the least magnesian eclogites. Thereby, the amphibolites with the lowest Mg content (MgO < 6 wt %) show the largest deviation from eclogite composition (Fig. 7). In particular, they have elevated Al_2O_3 and CaO contents and, in contrast, the lowest FeO and TiO_2 contents.

At narrow major-element variations, the studied rocks show wide trace-element variations (Fig. 8). Amphibolites demonstrate two types of REE distribution: LREE depleted $((La/Yb)_N$ 0.79–0.82) and LREE-enriched $((La/Yb)_N$ 2.31–2.99, $(La/Sm)_N$ 1.89–2.24) patterns relative to HREE (Fig. 8). Normalized HREE contents are 20–30 times chondrites, which are higher than typical N-MORB and E-MORB values. The exception is sample M16-42 with Yb_N ~ 14, which is lower than N-MORB value. All samples, except for sample M16-42, have Eu-minimum. Two samples (M16-36, M16-42) with massive structure and low content of epidote-clinozoisite display LREE depletion relative to HREE $((La/Yb)_N$ 0.79–0.82), LREE enriched or flat distribution pattern $((La/Sm)_N$ 0.83–1.09), and a weak negative Eu-anomaly (Eu/Eu* = 0.86–0.94) (Fig. 8a). The incompatible element distribution patterns (Fig. 8b) show positive Th, U, Nb-Ta, and Zr-Hf anomalies and negative Ti anomaly, as well as relative enrichment in large ion lithophile elements (Cs, Rb, and Ba). The distribution of other elements of this group differs in the considered samples. Amphibolite (sample M16-36) exhibits Sr and K minima and Pb maximum. In conrast, sample M16-42 has opposite (positive) K, Pb, and Sr anomalies.

In other samples (M16-37, M16-41, M16-43, M16-44) with variably expressed banding, the REE distribution pattern shows LREE enrichment compared to N-MORB and E-MORB (Fig. 8c) $((La/Yb)_N$ 2.31–2.99, $(La/Sm)_N$ 1.89–2.24), MREE enrichment relative to HREE with $(Sm/Yb)_N$ within 1.16–1.34, as well as Eu, Sr and Ti-minima, Th and U enrichment (except for one sample), and Nb and Ta enrichment relative to LREE (Fig. 8d), which is similar to that observed in sample M16-36 (Fig. 8b). In addition, there are negative K and Ba anomalies and positive Pb

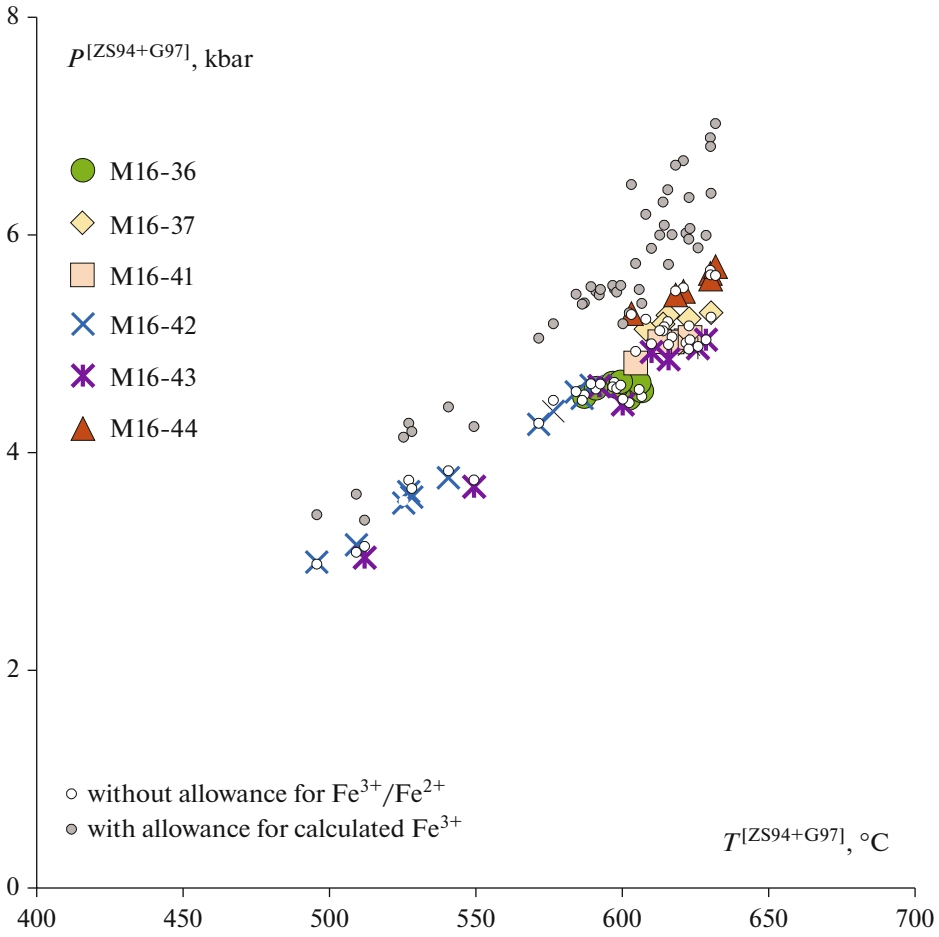

Fig. 6. *P-T* estimates for amphibolites based on the amphibole geothermobarometer (ZS94—Zenk and Schulz, 1994; G97—Gerya et al., 1997).

anomaly, except for sample M16-37 with Pb minimum.

Nd-Sr Isotope Composition

Amphibolites are characterized by a narrow range of $^{87}Sr/^{86}Sr$ (0.7057–0.7097) calculated for an age of 550 Ma (inferred age of accretionary events) at much wider variations of measured $^{87}Rb/^{86}Sr$ (0.0863–0.2756) (Table 3, Fig. 9). The Nd isotope composition shows wider variations of $\varepsilon_{Nd}(550)$ from +5.1 to –9.1. Corresponding values of model age T(DM) are plausible only for three samples (808–1418 Ma), whereas five of six samples yield close two-stage ages within 817–1134 Ma, and sample with the least radiogenic Nd composition yields the oldest model age of 1930 Ma.

DISCUSSION

Metamorphic Conditions

The studied amphibolites are made up of limited mineral associations, which for instance, in the absence of garnet, prevent the reliable temperature and pressure determination. The observed assemblages (high to moderate-Na plagioclase + epidote–clinozoisite + Ca-amphibole) in the absence of chlorite correspond to the high-pressure zone of the epidote–amphibolite and amphibolite facies (Maruyama et al., 1983; Starr et al., 2020). The moderate-Fe composition of epidote–clinozoisite in amphibolites ($X_{Fe^{3+}} < 0.25$) corresponds to that of amphibolite facies (Starr and Pattison, 2019), although depends on the degree of iron oxidation in the rock. It is noteworthy that the higher Fe^{3+} content in the outer zones of zonal epidote and some replaced domains indicates the growth/recrystallization of epidote–clinozoisite with decreasing temperature (Starr and Pattison, 2019) and/or the gradual growth of oxidizing potential at late low-temperature metamorphic stages (Raith, 1976; Keskinen and Liou, 1987). A potential role of decreasing temperature follows from compositional variations of amphibole and plagioclase, although it was difficult to estimate the equilibrium of definite amphibole with definite plagioclase in the studied

Table 2. Content of major (wt %) and trace (ppm) elements in the amphibolites of the Alag-Khadny Complex, SW Mongolia

Components	M16-36	M16-37	M16-41	M16-42	M16-43	M16-44
SiO_2	48.9	50.0	51.0	48.0	50.9	48.1
TiO_2	1.22	1.13	1.10	0.79	1.23	1.45
Al_2O_3	13.3	13.9	15.1	16.3	14.8	14.4
Fe_2O_3*	15.3	13.0	12.8	10.8	11.6	14.0
MnO	0.23	0.19	0.19	0.21	0.18	0.22
MgO	7.10	7.09	5.86	5.98	5.22	5.47
CaO	11.1	11.8	10.7	13.9	12.2	12.0
Na_2O	2.27	1.83	1.79	2.40	2.27	2.14
K_2O	0.19	0.24	0.54	0.35	0.51	0.71
P_2O_5	0.12	0.14	0.13	0.08	0.16	0.34
L.O.I.	0.78	1.29	1.4	1.67	1.49	1.11
Total	100.6	100.6	100.6	100.5	100.6	100.0
Cs	0.06	0.10	0.15	0.10	0.12	0.11
Rb	6.50	7.70	17.8	13.9	14.2	17.6
Ba	40.5	37.2	143	79.1	84.5	115
Th	1.12	2.60	2.88	0.34	1.75	4.54
U	0.31	0.72	0.79	0.12	0.60	1.16
Nb	8.10	20.3	8.36	3.13	14.1	30.3
Ta	0.53	1.27	0.54	0.19	0.83	1.88
La	5.85	13.2	13.4	2.51	10.9	22.8
Ce	13.3	28.0	27.5	5.97	23.7	47.8
Pb	1.48	1.66	3.81	1.24	4.73	5.58
Pr	1.91	3.63	3.58	0.92	3.14	6.00
Sr	127	261	199	172	215	182
Nd	9.37	15.5	14.6	4.91	14.0	24.7
Zr	90.0	134.0	90.0	50.0	94.0	190
Hf	2.62	3.84	2.26	1.42	2.51	5.30
Sm	3.36	4.35	3.72	1.89	3.77	6.40
Eu	1.15	1.25	1.06	0.71	1.34	1.59
Gd	5.00	5.45	4.63	2.77	4.72	7.71
Tb	0.96	0.97	0.81	0.53	0.81	1.33
Dy	6.80	6.42	5.42	3.49	5.40	8.73
Y	42.0	36.7	33.2	20.4	30.4	49.8
Ho	1.59	1.39	1.21	0.75	1.13	1.84
Er	4.98	4.12	3.67	2.38	3.32	5.52
Tm	0.72	0.60	0.54	0.32	0.48	0.79
Yb	4.83	3.82	3.48	2.17	3.21	5.19
Lu	0.72	0.57	0.53	0.32	0.48	0.77
V	483	351	255	303	335	385
Cr	71.4	132	124	350	130	80.7
Co	57.5	52.6	41.5	44.9	39.4	51.1
Ni	80.9	91.8	40.5	127	81.2	63.3
Cu	182	176	69.3	133	47.0	102
Zn	111	88.9	98.4	63.0	79.5	129
Ga	56.7	49.4	49.5	44.4	40.0	47.1

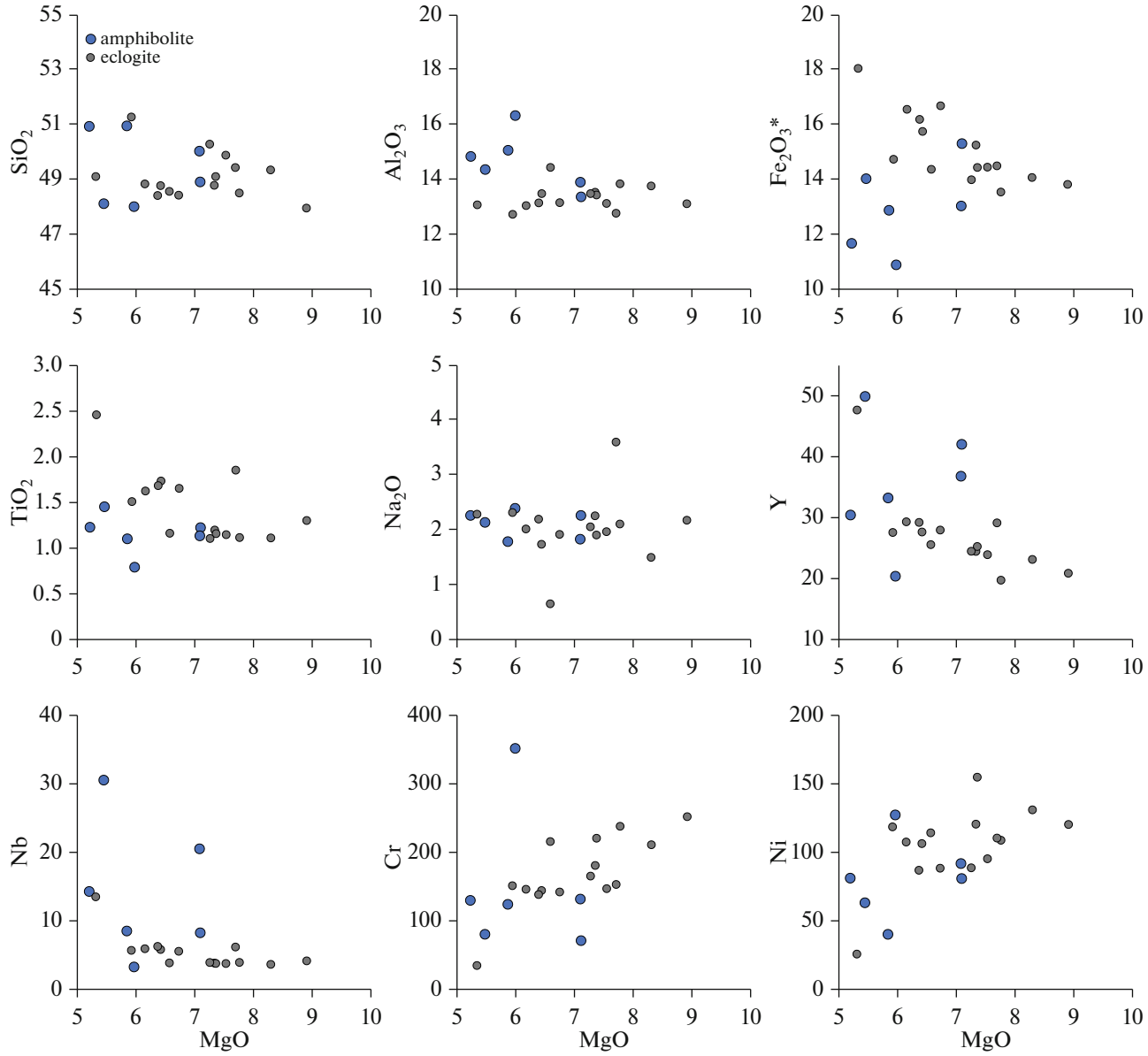

Fig. 7. Variations of some major (in wt %) and trace (in ppm) elements in the amphibolites. Compositions of eclogites from the Alag-Khadny Complex are shown for comparison (Skuzovatov et al., 2018).

amphibolites. Nevertheless, variation trends of two mineral phases suggest that the highest Al (^{IV}Al > 1.3 a.p.f.u) hornblende could be formed in equilibrium with the highest calcium (>20% anorthite) oligoclase–andesine at 600–650°C. Partial re-equilibration at lower temperatures in the epidote–amphibolite facies could occur in association of the highest-Na plagioclase with the highest-Si amphibole. The absence of tremolite–actinolite amphibole, which could be in equilibrium with albite as rims or separate grains/aggregates, could indicate the incompleteness of the process. In addition, the compositional variations of main rock-forming phases, including amphibole, plagioclase, and epidote–clinozoisite that accompany dissolution/reprecipitation deformations have been repeatedly described for medium-grade metamorphic rocks (e.g., Triboulet and Audren, 1988; Guintoli et al., 2018). Thus, intense deformation both in eclogites and in associated rocks could serve as catalysts for re-equilibration at retrograde stage.

Of great importance for deciphering the metamorphic evolution of amphibolites is the presence of indicators of high-pressure conditions such as garnet and rutile. In the studied amphibolites, Ti mineral carrier in most cases is titanite, however, in some cases, titanite is developed after rutile (Fig. 3f). The presence of rutile relicts in some amphibolites indicates that the rocks were subjected to high-pressure metamorphism,

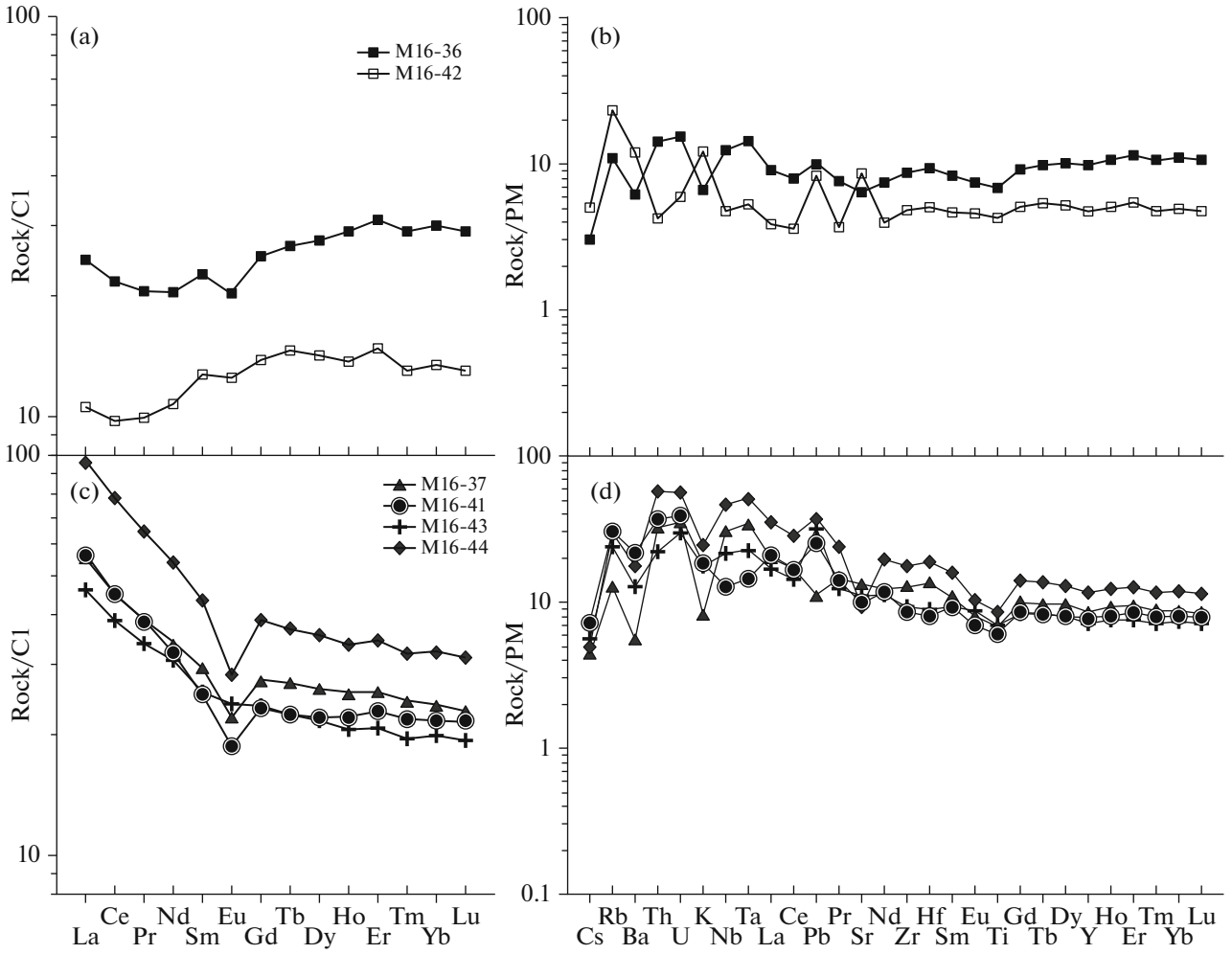

Fig. 8. Rare-earth element (a, c) and trace-element (b, d) patterns for amphibolites from the Alag-Khadny Complex. Element abundances are normalized to chondrite (C1) and primitive mantle (PM) compositions after (Sun and McDonough, 1989). Sample M16-41 (amphibolite) therein is shown by circle.

however, the definite boundaries of the rutile and titanite stability fields depend on the whole-rock composition, including Ca content (e.g., Frost et al., 2000), Mg#, as well as SiO_2 content. In particular, the rutile–titanite equilibrium in the medium-grade rocks according to (Kapp et al., 2009) is determined by garnet-bearing and garnet-free reactions:

$$2Czo/Zo + Rt + Qtz = 3An + Ttn + H_2O, \quad (1)$$

$$An + 2Ttn = Grs + 2Rt + Qz. \quad (2)$$

Table 3. Nd and Sr isotope composition in the amphibolites of the Alag Khadny Complex, SW Mongolia

Sample no.	Sr, ppm	Rb, ppm	$^{87}Rb/^{86}Sr$	$^{87}Sr/^{86}Sr$	±	Nd, ppm	Sm, ppm	$^{147}Sm/^{144}Nd$	$^{143}Nd/^{144}Nd$	±	$\varepsilon_{Nd}(550)$	Model age, Ma	
												T(DM)	T(DM-2st)
M-16-37	224	6.7	0.0863	0.70667	0.00002	15.1	4.05	0.16295	0.512570	0.000006	1.0	1402	1132
M-16-36	108	5.6	0.1504	0.70568	0.00002	10.0	3.49	0.21250	0.512893	0.000008	3.9	–	911
M-16-41	167	16.0	0.2756	0.70973	0.00002	14.2	3.48	0.14961	0.512000	0.000008	–9.1	–	1930
M-16-42	155	13.0	0.2482	0.70699	0.00001	6.21	2.28	0.2241	0.512996	0.000015	5.1	–	817
M-16-43	178	12.0	0.2003	0.70812	0.00002	13.1	3.51	0.16381	0.512572	0.000007	1.0	1418	1134
M-16-44	159	15.0	0.2656	0.70826	0.00002	24.6	4.24	0.10481	0.512493	0.000006	3.6	808	929

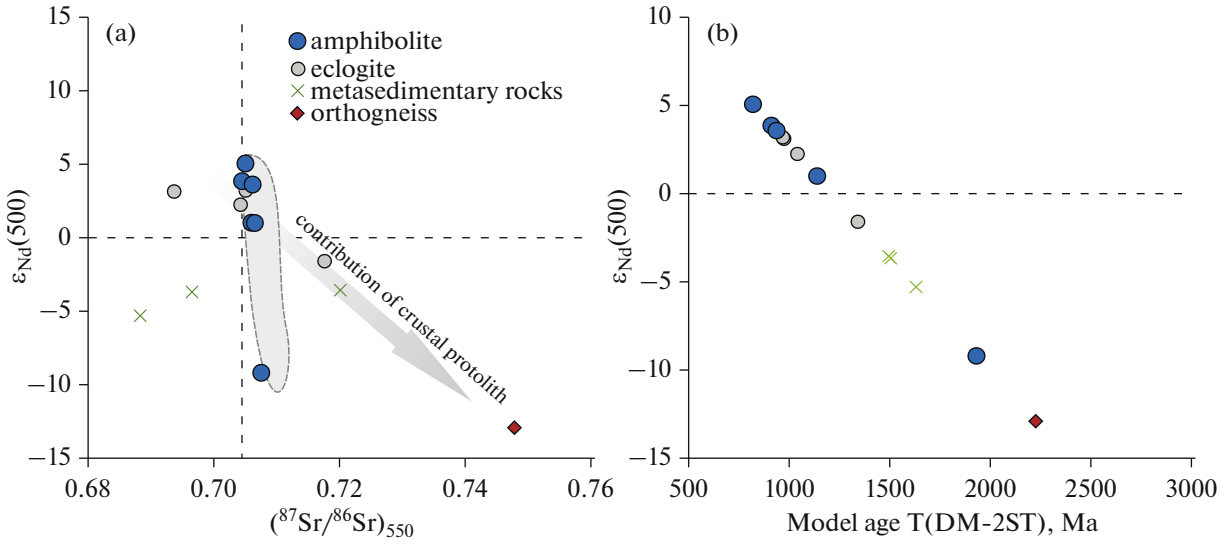

Fig. 9. The Nd and Sr isotope data on the studied amphibolites. The isotope characteristics of eclogites and associated felsic and metasedimentary rocks of the Alag-Khadny Complex are shown for comparison (Skuzovatov et al., 2018).

According to the experimental data on metamafic rocks (Oh and Liou, 1998; Kapp et al., 2009), the rutile–titanite transition in the medium-temperature region (500–700°C) occurs within 12–14 kbar, and, hence, titanite could be the product of retrograde transformation of higher pressure rocks. Nevertheless, *P-T* modeling for the average MOR basalts and particular basalts of the similar composition points to the appearance of rutile at the same moderate to high temperatures of 500–700°C, but at much lower pressures of 7–8 kbar (Starr et al., 2019). Similar results are consistent with thermobarometric estimates on the epidote–clinozoisite amphibolites (Kapp et al., 2009), which revealed that *P-T* equilibrium conditions of the rutile-bearing amphibolites widely vary (~500–780°C, 7–12 kbar) and are significantly overlapped with *P-T* parameters determined for titanite-bearing rocks (~500–650°C, 5–11 kbar). Thus, rutile relicts found in the titanite cores of some studied samples could indicate the pressure more than 5–7 kbar, which is consistent with peak *P-T* conditions determined from amphibole–plagioclase assemblages (likely, up to ~7 kbar and no more than ~650°C). Presented literature data indicate that the higher *P-T* parameters, in particular, higher pressure, are not required for rutile formation. The garnet stability field in the amphibolites is usually wider than the rutile field and is extended to the relatively lower pressure region. At the same time, the appearance of garnet in MOR-type basalts at ~500–800°C is related to reactions involving low-temperature amphibole and epidote–clinozoisite at transition from epidote–amphibolite to eclogite facies at ~8–10 kbar (e.g., Ernst and Liu, 1998; Oh and Liou, 1998; Starr et al., 2020), which is even slightly higher than values typical of rutile. Thus, the absence of garnet relicts or its low-pressure pseudomorphs in the observed assemblages (e.g., plagioclase–hornblende or quartz–clinozoisite) in the presence of rutile relicts suggests metamorphic evolution of rocks at pressure no more than ~7 kbar.

Based on calculations of *P-T* metamorphic parameters, the amphibolites from the Alag-Khadny Complex had distinct Barrovian-type metamorphic evolution different from eclogite evolution, but they do not contain mineralogical indicators of high-pressure metamorphism. At the same time, Javkhlan et al. (2019) showed that metamorphism of eclogites of the Alag-Khadny Complex could occur in two stages. The final accretionary/collisional stage produced garnet amphibolites (*Grt* + An_{1-13} + Mg-*Hbl* + *Ep*) at ~550–610°C and 7–8 kbar, with subsequent cooling and decompression up to the greenschist facies conditions (*Chl* + *Ab* + *Ep* + *Act*). However, the equilibrium state of the garnet causes some doubts: eclogite garnet in the rocks has characteristic prograde zoning with outward increase of X_{Mg} and decrease of X_{Ca} and a change of mineral assemblage of the inclusions from hydrous (clinozoisite/epidote, amphibole) to anhydrous (quartz, rutile, omphacite), which excludes the growth, dissolution/precipitation, or noticeable diffusion re-equilibration of garnets owing to the late thermal event. Hence, the high-Na plagioclase + hornblende + epidote/clinozoisite assemblage similar in conditions to those of the studied amphibolites implies that the amphibolites and retrograded eclogites shared a common *P-T* evolution.

Nature of Geochemical Variations

In spite of a limited number of the studied samples, amphibolites reveal significant geochemical and isotope variations. Their incompatible element distribu-

tion patterns are similar: multielement diagrams for amphibolites (Figs. 8b, 8d), except for the most depleted amphibolite sample M16-36, are characterized by the enrichment in Th and U relative to large-ion lithophile elements, which is not typical of N-MORB and E-MORB oceanic basalts, Pb-maximum (except for one sample), and Nb and Ta enrichment relative to LREE typical of E-MORB (except for one sample). Thereby, amphibolites have different contents of the considered elements. Such significant variations can be caused by (1) juxtaposition of rocks of initially different composition (from depleted N-MORB type to enriched E-MORB-type and continental basalts) within accretionary structure, (2) crustal contamination of melts, (3) fractionation of melts or combination of two above factors.

The amphibolites have nearly MORB values of TiO_2 content (~1.5 wt %), as well as nearly N-MORB values of SiO_2 (within 49–51 wt %) and Na_2O (~2 wt %) contents at systematically higher FeO content (>11 wt %) (Fig. 7). The Mg# of the rocks is lower than that of primitive MORB melts (Mg# 47.3–52.3). Hence, their compositions do not correspond to primary primitive melts and could be formed by fractionation of melts during crystallization of olivine, plagioclase, and Ti-magnetite. This could result in the high HREE and negative Eu and Ti anomalies in the rocks. Compared to other rocks, protolith of amphibolite (sample M16-42) could be enriched in low-REE mineral, for instance, in plagioclase. This is confirmed by the high Al_2O_3 content in the rock and positive Rb and Sr anomalies, whereas the absence of the positive Eu anomaly could be related to the intrusive rather than effusive nature of amphibolite protolith.

The amphibolites have significant variations of large-ion lithophile elements expressed in values of the Sr/Nb and Rb/Sr ratios (Figs. 10c, 10d), as well as less mobile elements, for instance, Th or LREE (Figs. 10a, 10b). In the medium-grade metamorphic rocks, the large-ion lithophile elements are partitioned between plagioclase and amphibole, while Sr is mainly partitioned in plagioclase. The majority of the studied amphibolites contain plagioclase of two generations: anorthite-rich ($X_{An} > 0.2$) and albite with K_2O admixture, which partially (as rims) or completely replaces initial plagioclase (Fig. 5b). It has been repeatedly shown that the transformation of oceanic crust rocks under low-temperature conditions up to the greenschist facies could lead to the loss of Sr and other fluid-mobile elements owing to the replacement of primary magmatic or higher temperature metamorphic, anorthite-rich plagioclase (e.g., Kirchner and Gillis, 2012). Thus, Rb and Sr variations could be caused by the transformation of initial high- to moderate-Ca plagioclase and reflect the mobility of large-ion lithophile elements during both fluid metasomatism of protolith and retrograde transformation of amphibolites.

Discriminant diagrams based on the content of elements that are inert during metamorphism (Pearce, 2014; Saccani, 2015) allowed us to class all amphibole samples with tholeiitic basalts (Fig. 11a). In the Th_N–Nb_N diagram (Fig. 11b), composition points of the amphibolites fall in the oceanic basalt field, with LREE-depleted amphibolites falling in the N-MORB field, and LREE-enriched amphibolites, in the E-MORB and P-MORB overlap. Additional normalization of trace-element contents to $Yb_{N\text{-}MORB}$ makes it possible to minimize the fractionation effect (Pearce et al., 2021) and indicates the affinity of LREE-depleted amphibolites to N-MORB in terms of all their characteristics except for Th and U enrichment (Fig. 12a). The enrichment of amphibolites in inert Th, Nb, and Ta should reflect the composition of source rocks during formation of their protoliths. Thus, the protoliths of depleted amphibolites could not be formed only from depleted mantle source. The N-MORB- and $Yb_{N\text{-}MORB}$-normalized compositions of LREE-enriched amphibolites in the Alag-Khadny complex (samples M16-37, M16-43, and M16-44) are similar to E-MORB, in particular, to composition of tholeiitic basalts from the Sarve-Abad ophiolite complex (Iran) (Saccani et al., 2014), except for the higher Th and U contents (Fig. 12b). These rocks show no any prograde contribution of typical crustal enriched component. At the same time, according to used discrimination models, the eclogites of the Alag-Khadny Complex most resemble the N-MORB and G-MORB basalts (Figs. 11–13).

Contamination of mafic MORB-like melts by crustal protolith would result in the negative anomalies of high-field strength elements (first of all, Nb-Ta and Ti) relative to REE and corresponding increase, in particular, of Th/La, La/Nb, and Sr/Nb ratios, which is not observed in the studied rocks (Figs. 10a–10c). This is confirmed by the absence of correlation between Nd isotope composition and above-mentioned ratios in the studied rocks, and, in contrast, the radiogenic Nd composition of the highest LREE amphibolites (for instance, in sample M16-44). In addition, the low alkalinity and Ti content in the amphibolites are also not typical of continental tholeiites. Thus, the systematically elevated contents of large ion lithophile elements, Th, and U, can be partially inherited from primary melts. At the same time, some samples of eclogites and amphibolites have higher Th/Nb ratio compared to MORB (Pearce et al., 2021), and a few samples demonstrate negative Nb–Ta anomalies and unradiogenic Nd isotope composition ($\varepsilon_{Nd}(T) < 0$). Such features could be explained by the crustal contamination of primary melts. In addition, the enrichment of amphibolites and eclogites of all distinguished geochemical types in Th, U, and, to different extent, in Nb and Ta compared to MORB-type mafic rocks indicates a potential involvement of lithospheric mantle in melting.

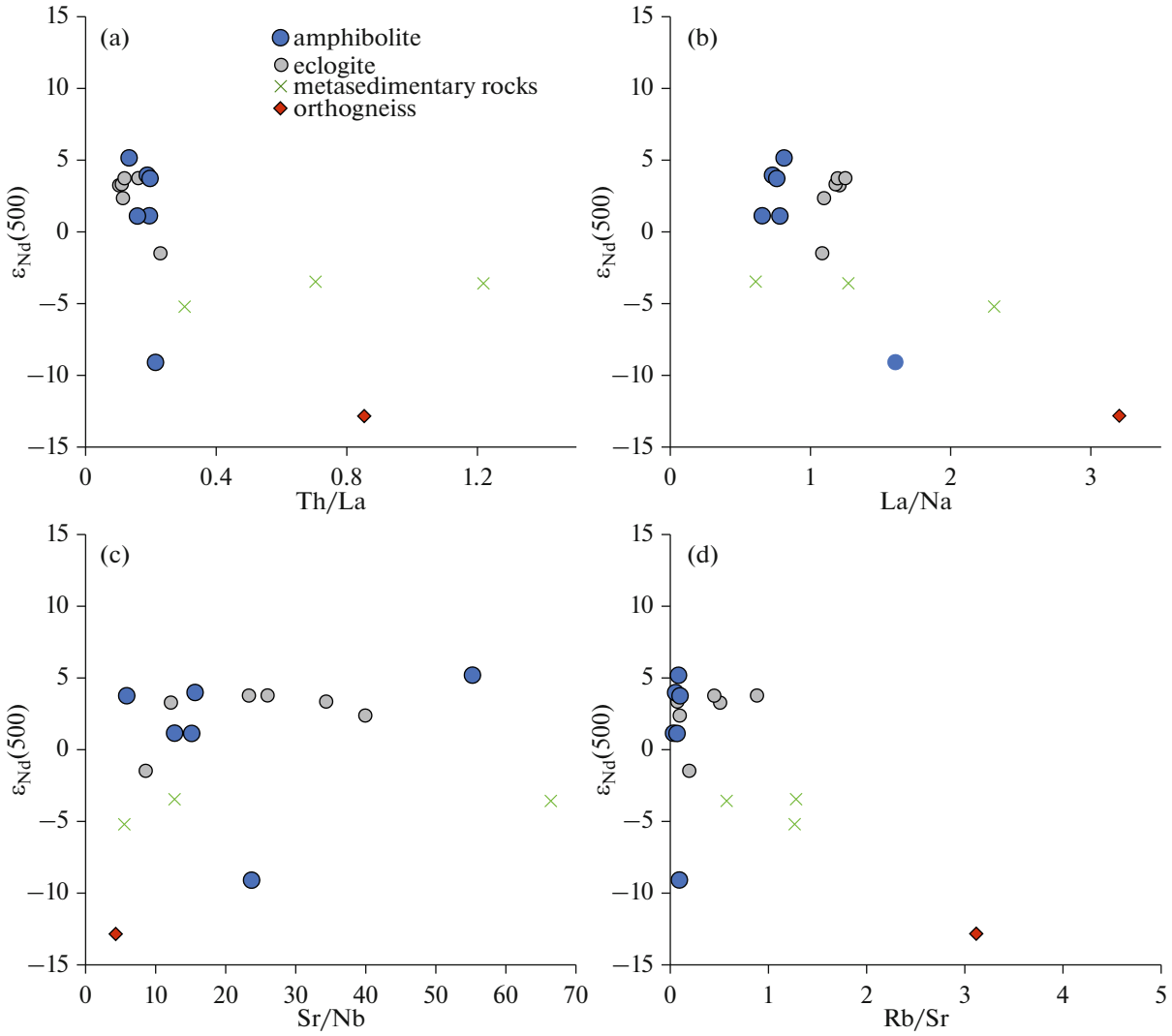

Fig. 10. Covariations of Nd isotope characteristics and indicator element ratios in the amphibolites (this study) and in high-pressure rocks of the Alag-Khadny Complex (Skuzovatov et al., 2018).

Geodynamic Setting of the Formation of Amphibolite Protolith and Relationship with High-Pressure Rocks in the Accretionary System of SW Mongolia

The Alag-Khadny accretionary complex comprises association of metamorphic rocks, whose protoliths could be generated from N-MORB, G-MORB, and E-MORB-type melts at predominant melting of asthenospheric depleted and enriched mantle, respectively. The principal difference of reconstructed eclogite protolith from amphibolite protolith is variations between N-MORB and G-MORB compositions (Fig. 13), and to lesser extent, between E-MORB and P-MORB-type enriched basalts (Figs. 11, 12). The MREE enrichment relative to HREE in G-MORB basalts is interpreted as a result of melting of garnet-bearing mantle source (e.g., Montanini et al., 2008). This suggests that melting involved the deeper seated (garnet peridotite) mantle facies or likely metasomatized (garnet–pyroxenite) mantle domains among typical spinel peridotites (Saccani et al., 2015), which generate most MORB-type melts (Niu, 1997). The enrichment in Nb and other incompatible elements relative to N-MORB observed in the amphibolites is typical of E-MORB-type mafic rocks related to the variable involvement of mantle domains metasomatized by asthenospheric/lower mantle or subduction melts (Gale et al., 2013 for overview). According to (Castillo et al., 2002), volcanic rocks formed in the axial parts of extension zones during continental rifting could have more enriched and evolved composition relative to N-MORB, as is observed for the studied amphibolites. In recent classification, Dilek and Furnes (2014) describes the continental-margin ophiolites representing fragments of newly formed oceanic crust of N-MORB, G-MORB, and E-MORB types of the ocean–continent transition zone, which was

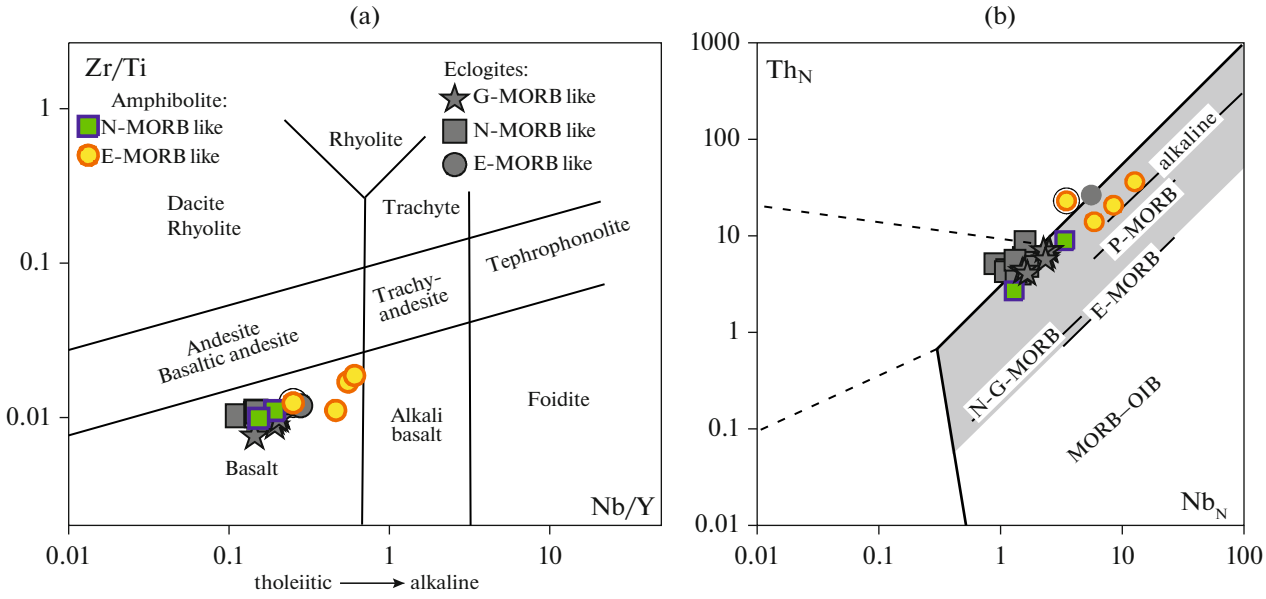

Fig. 11. (a) Zr/Ti–Nb/Y classification diagram for volcanic rocks (Pearce, 2014). (b) Th_N–Nb_N discrimination diagram after (Saccani, 2015). The values were normalized to N-MORB after (Sun, McDonough, 1989). Gray field—oceanic basalts.

formed during continent breakup. Hence, the protolith of the eclogites and amphibolites could be formed within a single riftogenic passive margin, as was proposed for spatially juxtaposed N-MORB, T-MORB, and E-MORB type rocks (Andreasson and Albrecht, 1995).

Isotope-geochemical features of most amphibolites and eclogites of the Alag-Khadny Complex indicate a moderately depleted mantle source of parental melts. This is consistent with an extensional setting and formation of oceanic crust, but cannot explain the existence of rocks with unradiogenic Nd ($\varepsilon_{Nd}(T) < 0$) composition among amphibolites (Figs. 9, 10, Table 3) and eclogites (Skuzovatov et al., 2018). Corresponding $\varepsilon_{Nd}(T)$ values could be interpreted as reflecting the crustal contamination or interaction with a crustal fluid during amphibolization (Fig. 9). However, the isotope characteristics do not correlate with geochemical signatures of crustal contribution and, in general, correspond to the end compositions of E-MORB, for instance, those of the Indian Ocean (e.g., White and Klein, 2014).

A spatial association of amphibolites with carbonate mélange bearing Cambrian fauna (Kröner et al., 2010), unlike mainly Early Neoproterozoic (Tonian) and Mesoproterozoic ages of crystalline rocks of the Alag-Khadny and Zamtyn-Nuruu complexes (Buriánek et al., 2017; Skuzovatov, 2021), indicates a possible relation of protolith of amphibolites and eclogites with close model Nd ages (T(DM) ~ 1500–800 Ma) with Neoproterozoic rifting of yet undetermined age (~900–540 Ma). According to model proposed in (Skuzovatov et al., 2018), the formation of eclogite protolith was related to rifting of passive continental margin and opening of a limited oceanic basin, which is supported by the absence of conjugate fragments of oceanic or island-arc ophiolites. Thus, geochemically and isotopically heterogenous protoliths of N-MORB and E-MORB-type amphibolites could represent a missing fragment of this riftogenic association.

All available *P-T* estimates for eclogites and associated metagranitoids and metasedimentary rocks indicate subduction and accretionary/collisional metamorphic trends during subsequent change of tectonic regime that accompanied the closure of the limited oceanic basin. The absence of evidence for high-pressure metamorphic conditions suggests that the amphibolite protolith did not experienced subduction eclogite metamorphism, but could be involved in medium to elevated-pressure accretionary metamorphism in the Late Ediacaran–Early Cambrian, which is marked by ^{40}Ar-^{39}Ar age of high-pressure rocks (Štípská et al., 2010) and age of metamorphic zircons from metagranitoids and metasedimentary rocks (Buriánek et al., 2017; Skuzovatov, 2021). Note that the considered metamorphic complexes are restricted to the junction zone of the Early Caledonian Lake Zone and Dzabkhan terrane. This zone consists of tectonic nappes of different age (from Paleoproterozoic, Early and Neoproterozoic to Early Paleozoic) made up of granulite to amphibolite facies rocks (Kozakov et al., 2021; Bold et al., 2016; Buriánek et al., 2017; Kröner et al., 2010). The upper age limit of metamorphism in the indicated blocks in the different parts of the mélange zone is constrained by ~515–490 Ma. Hence, the mélange zone was formed after completion of the Early Paleozoic metamorphism within this time interval.

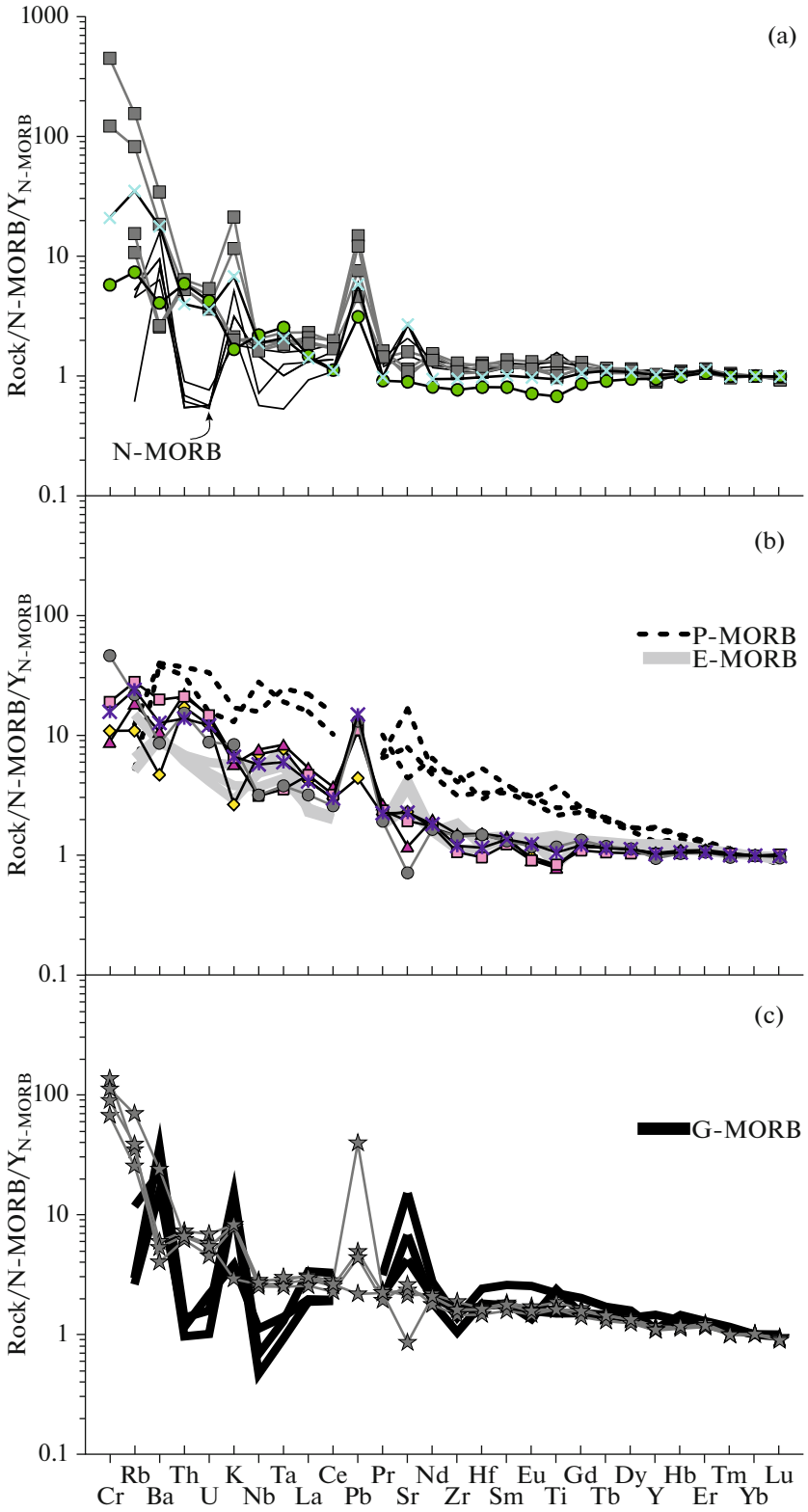

Fig. 12. Yb- and N-MORB-normalized multielement diagrams for the amphibolites and eclogites of the Alag-Khadny Complex. For symbols, see Fig. 11. Compositions of N-, P-, E- and G-MORB volcanic rocks from the Sarve-Abad ophiolite complex are shown for comparison (Saccani et al., 2014).

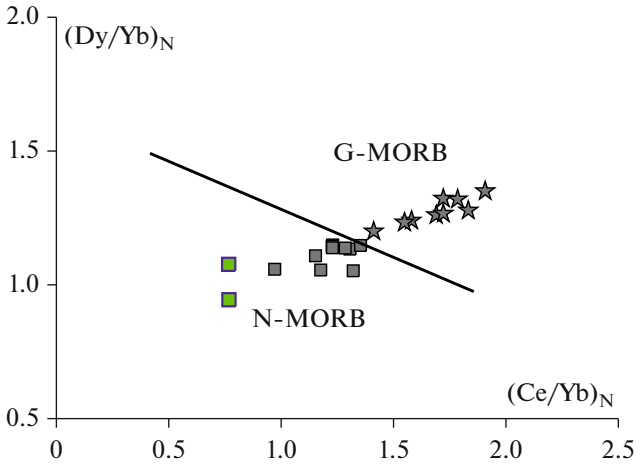

Fig. 13. Separation of the N- and G-MORB volcanic rocks in the Dy/Yb–Ce/Yb discrimination diagram after (Saccani et al., 2015). The values are normalized to C1 chondrite (Sun and McDonough, 1989). For symbols, see Fig. 11.

CONCLUSIONS

Obtained data indicate that the Alag-Khadny accretionary complex comprises association of high- and medium-pressure rocks with geochemical signatures of N-MORB, G-MORB, and E-MORB, which are typical of ophiolite complexes of the ocean–continent transition zone. Given their spatial association with two gneiss complexes of similar age, Alag-Khadny and Zamtyn-Nuruu (~960–950 Ma), the protolith of the amphibolites and eclogites was likely formed in an intracontinental extension setting related to the formation of a limited Neoproterozoic oceanic basin and subsequent Late Vendian–Early Caledonian convergence. At the absence of reliable geochronological data, we suggest that the medium-high pressure metamorphism, which formed amphibolites of the indicated geochemical affinity and was similar in *P-T* parameters with retrograde metamorphism of eclogites and associated metasedimentary rocks, was related to the accretionary processes responsible for the Early Paleozoic subduction–accretion metamorphism (~550–540 Ma) or resulted from final accretion with formation of tectonic mélange zone between the Lake Zone and Dzabkhan terrane (~515–490 Ma and younger).

ACKNOWLEDGMENTS

We are grateful to P.Ya. Azimov and I.K. Kozakov for valuable comments and suggestions, which allowed us to improve interpretation and presentation of materials.

FUNDING

The studies were performed in the framework of the government-financed task of the Vinogradov Institute of Geochemistry, Siberian Branch, Russian Academy of Sciences (project nos. 0284-2021-0007 and 0284-2021-0006) and were supported by the Russian President Foundation (project MK-67.2020.5).

CONFLICT OF INTEREST

The authors declare that they have no conflicts of interest.

SUPPLEMENTARY INFORMATION

The online version contains supplementary material available at https://doi.org/10.1134/S0869591122040051.

REFERENCES

Andreasson, P.-G. and Albrecht, L., Derivation of 500 Ma eclogites from the passive margin of Baltica and a note on the tectonometamorphic heterogeneity of eclogite-bearing crust, *Geol. Mag.,* 1995, vol. 132, no. 6, pp. 729–738.

Bold, U., Crowley, J.L., Smith, E.F., et al., Neoproterozoic to Early Paleozoic tectonic evolution of the Zavkhan terrane of Mongolia: implications for continental growth in the Central Asian Orogenic Belt, *Lithosphere,* 2016, vol. 8, no. 6, pp. 729–750.

Brown, E.H., The crossite content of Ca-amphibole as a guide to pressure of metamorphism, *J. Petrol.,* 1977, vol. 18, pp. 53–72.

Buriánek, D., Schulmann, K., Hrdličkova, K., et al., Geochemical and geochronological constraints on distinct Early Neoproterozoic and Cambrian accretionary events along southern margin of the Baydrag continent in Western Mongolia, *Gondwana Res.,* 2017, vol. 47, pp. 200–227.

Castillo, P.R., Hawkins, J.W., Lonsdale, P.F., et al., Petrology of Alarcon rise lavas, Gulf of California: nascent intracontinental ocean crust, *J. Geophys. Res.,* 2002, vol. 107, p. 2222.

Dilek, Y. and Furnes, H., Ophiolites and their origins, *Elements,* 2014, vol. 10, pp. 93–100.

Dobretsov, N.L., Buslov, M.M., and Vernikovsky, V.A., Neoproterozoic to Early Ordovician evolution of the paleo-Asian ocean: implications to the break-up of Rodinia, *Gondwana Res.,* 2003, vol. 6, no. 2, pp. 143–159.

Ernst, W.G. and Liu, J.G., Experimental phase–equilibrium study of Al- and Ti-contents of calcic amphibote in MORB - a semiquantitative thermobarometer, *Am. Mineral.,* 1998, vol. 83, pp. 952–969.

Ernst, W.G., Alpine and Pacific styles of Phanerozoic mountain building: subduction-zone petrogenesis of continental crust, *Terra Nova,* 2005, vol. 17, pp. 165–188.

Frost, B.R., Chamberlain, K.R., and Schumacher, J.C., Sphene (titanite): phase relations and role as a geochronometer, *Chem. Geol.,* 2000, vol. 172, pp. 131–148.

Gale, A., Dalton, C.A., Langmuir, C.H., et al., The mean composition of ocean ridge basalts, *Geochem. Geophys. Geosyst.,* 2013, vol. 14, pp. 489–518.

Gerya T.V., Perchuk L.L., Tribule K., et al., Petrology of the Tumanshet zonal metamorphic complex, Eastern Sayan, *Petrology,* 1997, vol. 5, no. 6, pp. 503–533.

Gornova, M.A., Karimov, A.A., Skuzovatov, S.Yu., and Belyaev, V.A., From decompression melting to mantle-wedge refertilization and metamorphism: insights from peridotites of the Alag-Khadny accretionary complex (SW Mongolia), *Minerals,* 2020, vol. 10, no. 5, p. 396.

Guintoli, F., Menegon, L., and Warren, C.J., Replacement reactions and deformation by dissolution and precipitation processes in amphibolites, *J. Metamorph. Geol.,* 2018, vol. 36, pp. 1263–1286.

Hanžl, P. and Aichler, J., *Geological survey of the Mongolian Altay at a scale 1 : 50000 (Zamtyn Nuruu—50). Final report, Czech Geological Survey,* Prague: Czech Republic, 2007.

Hawthorne, F.C., Oberti, R., Harlow, G.E., et al., Nomenclature of the amphibole supergroup, *Am. Mineral.,* 2012, vol. 97, pp. 2031–2048.

Holland, VOL. and Blundy, J., Non-ideal interactions in calcic amphiboles and their bearing on amphibole-plagioclase thermometry, *Contrib. Mineral. Petrol.,* 1994, vol. 116, pp. 433–447.

Jahn, B.-M., Wu, F., and Chen, B., Granitoids of the Central Asian Orogenic Belt and continental growth in the Phanerozoic, *Trans. R. Soc. Edinburgh: Earth Sci.,* 2000, vol. 91, pp. 181–193.

Javkhlan, O., Takasu, A., Fazle, KabirMd., and Batulzii, D., Multiple metamorphic events recorded within eclogites of the Chandman District, SW Mongolia, *Minerals,* 2019, vol. 9, p. 495.

Kapp, P., Manning, C.E., and Tropper, P., Phase-equilibrium constraints on titanite and rutile activities in mafic epidote amphibolites and geobarometry using titanite–rutile equilibria, *J. Metamorph. Geol.,* 2009, vol. 27, pp. 509–521.

Keskinen, M. and Liou, J.G., Stability relations of Mn–Fe–Al piemontite, *J. Metamorph. Geol.,* 1987, vol. 5, pp. 495–507.

Khain, E.V., Bibikova, E.V., Salnikova, E.E., et al., The paleo-Asian ocean in the Proterozoic and Early Paleozoic: new geochronologic data and paleotectonic reconstructions, *Precambrian Res.,* 2003, vol. 122, pp. 329–358.

Kirchner, T.M. and Gillis, K.M., Mineralogical and strontium isotopic record of hydrothermal processes in the lower ocean crust at and near the east pacific rise, *Contrib. Mineral. Petrol.,* 2012, vol. 164, pp. 123–141.

Kozakov, I.K., Kovach, V.P., Salnikova, E.B., et al., Formation of the Neoproterozoic continental crust in the structures of the central segment of the Central Asian Fold Belt, *Petrology,* 2021, vol. 29, no. 2, pp. 195–220.

Kozakov, I.K., Salnikova, E.B., Wang, T., et al., Early Precambrian crystalline complexes of the Central Asian microcontinent: age, sources, tectonic position, *Stratigraphy. Geol. Correlation,* 2007, vol. 15, no. 2, pp. 121–140.

Kozakov, I.K., Yarmolyuk, V.V., Kovach, V.P., et al., The Early Baikalian crystalline complex in the basement of the Dzabkhan microcontinent of the Early Caledonian orogenic area, Central Asia, *Stratigraphy. Geol. Correlation,* 2012, vol. 20, no. 3, pp. 3-12.

Kröner, A., Lehmann, J., Schulmann, K., et al., Lithostratigraphic and geochronological constraints on the evolution of the Central Asian Orogenic Belt in SW Mongolia: Early Paleozoic rifting followed by Late Paleozoic accretion, *Am. J. Sci.,* 2010, vol. 310, pp. 523–574.

Laird, J. and Albee, A.L., Pressure, temperature, and time indicators in mafic schist: their application to reconstructing the polymetamorphic history of Mermont, *Am. J. Sci.,* 1981, vol. 281, pp. 127–175.

Locock, A.J., An excel spreadsheet to classify chemical analyses of amphiboles following the IMA 2012 recommendations, *Comp. Geosci.,* 2014, vol. 62, pp. 1–11.

Maruyama, S., Suzuki, K., and Liou, J., Greenschist-amphibolite transition equilibria at low pressures, *J. Petrol.,* 1983, vol. 24, pp. 583–604.

Matsumoto, I. and Tomurtogoo, O., Petrological characteristics of the Pantaishir ophiolite complex, Altai region, Mongolia: coexistence of podiform chromitite and boninite, *Gondwana Res.,* 2003, vol. 6, pp. 161–169.

Montanini, A., Tribuzio, R., and Vernia, L., Petrogenesis of basalts and gabbros from an ancient continent–ocean transition (external Liguride ophiolites, northern Italy), *Lithos,* 2008, vol. 101, pp. 453–479.

Niu, Y., Mantle melting and melt extraction processes beneath ocean ridges: evidence from abyssal peridotites, *J. Petrol.,* 1997, vol. 38, no. 8, pp. 1047–1074.

Oh, C.W. and Liou, J.G., A petrogenetic grid for eclogite and related facies under high-pressure metamorphism, *The Island Arc,* 1998, vol. 7, pp. 36–51.

Pearce, J.A., Immobile element fingerprinting of ophiolites, *Elements,* 2014, vol. 10, pp. 101–108.

Pearce, J.A., Ernst, R.E., Peate, D.W., and Rogers, C., LIP printing: use of immobile element proxies to characterize large igneous provinces in the geologic record, *Lithos,* 2021, p. 1016.
https://doi.org/10.1016/j.lithos.2021.106068

Raase, P., Al and Ti contents of hornblende, indicators of pressure and temperature of regional metamorphism, *Contrib. Mineral. Petrol.,* 1974, vol. 45, pp. 231–236.

Raith, M., The A1–Fe(III) epidote miscibility gap in a metamorphic profile through the Penninic series of the Tauern window, Austria, *Contrib. Mineral. Petrol.,* 1976, vol. 57, pp. 99–117.

Rudnev, S.N., Kovach, V.P., and Ponomarchuk, V.A., Vendian–Early Cambrian island-arc plagiogranitoid magmatism in the Altai–Sayan folded area and in the Lake Zone of Western Mongolia (geochronological, geochemical and isotope data), *Russ. Geol. Geophys.,* 2013, vol. 54, no. 10, pp. 1272–1287.

Saccani, E., Allahyari, K., and Rahimzadeh, B., Petrology and geochemistry of mafic magmatic rocks from the Sarve-Abad ophiolites (Kurdistan region, Iran): evidence for interaction between MORB-type asthenosphere and OIB-type components in the southern Neo-Tethys Ocean, *Tectonophysics,* 2014, vol. 621, pp. 132–147.

Saccani, E., Dilek, Y., Marroni, M., and Pandolfi, L., Continental margin ophiolites of Neotethys: remnants of ancient ocean-continent transition zone (OCTZ) lithosphere and their geochemistry, mantle sources and melt evolution patterns, *Episodes,* 2015, vol. 38, pp. 230–249.

Saccani, E., A new method of discriminating different types of post-Archean ophiolitic basalts and their tectonic significance using Th–Nb and Ce–Dy–Yb systematics, *Geosc. Front.,* 2015, vol. 6, pp. 481–501.

Schumacher, J.C., Metamorphic amphiboles: composition and coexistence, *Rev. Mineral. Geochem.,* 2007, vol. 67, pp. 359–416.

Sengör, A.M.C., Natal'in, B.A., and Burtman, V.S., Evolution of the Altaid tectonic collage and Paleozoic crustal growth in Eurasia, *Nature,* 1993, vol. 364, pp. 299–307.

Skuzovatov, S.Yu., Nature and (in-)coherent metamorphic evolution of subducted continental crust in the Neoproterozoic accretionary collage of SW Mongolia, *Geosci. Front.,* 2021, vol. 12, no. 3, p. 101097.

Skuzovatov, S.Yu., Shatsky, V.S., Dril, S.I., and Perepelov, A.B., Elemental and isotopic (Nd–Sr–O) geochemistry of eclogites from the Zamtyn-Nuruu area (SW Mongolia): crustal contribution and relation to Neoproterozoic subduction–accretion events, *J. Asian Earth Sci.,* 2018, vol. 167, pp. 33–51.

Song, S., Zhang, L., Niu, Y., Su, L., et al., Evolution from oceanic subduction to continental collision: a case study from the northern Tiberan plateau based on geochemical and geochronological data, *J. Petrol.,* 2006, vol. 47, no. 3, pp. 435–455.

Spear, F.S., NaSi-CaAl exchange equilibrium between plagioclase and amphibole: an empirical model, *Contrib. Mineral. Petrol.,* 1980, vol. 80, pp. 140–149.

Starr, P.G. and Pattison, D.R.M., Equilibrium and disequilibrium processes across the greenschist—amphibolite transition zone in metabasites, *Contrib. Mineral. Petrol.,* 2019, vol. 174, no. 2, pp. 1–18.

Starr, P.G., Pattison, D.R.M., and Ames, D.E., Mineral assemblages and phase equilibria of metabasites from the prehnite–pumpellyite to amphibolite facies, with the Flin Flon greenstone belt (Manitoba) as a type example, *J. Metamorph. Geol.,* 2020, vol. 38, pp. 71–102.

Štípská, P., Schulmann, K., Lehmann, J., et al., Early Cambrian eclogites in SW Mongolia: evidence that the palaeo-Asian ocean suture extends further than expected, *J. Metamorph. Geol.,* 2010, vol. 28, pp. 915–933.

Sun, S.-S. and McDonough, W.F., *Chemical and isotopic systematics of oceanic basalts: implications for mantle composition and processes, Magmatism in the Ocean Basins,* Saunders, A.D. and Norry, M.J., Eds., *Geol. Soc. Spec. Publ.,* 1989, vol. 42, pp. 313–345.

Tomurtogoo, O., A new tectonic scheme of the Paleozoides in Mongolia, *Mongol. Geosci.,* 1997, vol. 3, pp. 12–17.

Triboulet, C. and Audren, C., Controls on *P-T*-t deformation path from amphibole zonation during progressive metamorphism of basic rocks (estuary of the River Vilaine, South Brittany, France), *J. Metamorph. Geol.,* 1988, vol. 6, pp. 117–133.

White, W.M. and Klein, E.M., *Composition of the oceanic crust*, *Treatise on Geochemistry,* 2nd Ed., 2014, vol. 4, pp. 457–496.

Whitney, D.L. and Evans, B.W., Abbreviations for names of rock-forming minerals, *Am. Mineral.,* 2010, vol. 95, pp. 185–187.

Yarmolyuk V.V., Kovalenko V.I., Kovach V.P., et al., Early stages of the Paleoasian ocean formation: results of geochronological, isotopic, and geochemical investigations of Late Riphean and Vendian–Cambrian complexes in the Central Asian Foldbelt, *Dokl. Earth Sci.,* vol. 410, no. 5, pp. 1184–1189.

Zenk, M. and Schulz, B., Zoned Ca-amphiboles and related *P-T* evolution in metabasites from the classical Barrovian metamorphic zones in Scotland, *Mineral. Mag.,* 2004, vol. 68, no. 5, pp. 769–786.

Zhang, G., Zhang, L., and Christy, A.G., From oceanic subduction to continental collision: an overview of HP–UHP metamorphic rocks in the North Qaidam UHP belt, NW China, *J. Asian Earth Sci.,* 2013, vol. 63, pp. 98–111.

Translated by M. Bogina